POWDER MIXED EDM FOR BIOMEDICAL ALLOYS

Nurlan Nauryz, B.Eng. in Mechanical Engineering

Submitted in fulfillment of the requirements
for the degree of Master of Science
in Mechanical & Aerospace Engineering

NAZARBAYEV UNIVERSITY

School of Engineering and Digital Sciences
Department of Mechanical & Aerospace Engineering
Nazarbayev University
53 Kabanbay Batyr Avenue,
Astana city, Kazakhstan, 010000

Supervisor: Assistant Professor Asma Perveen
Co-supervisor: Associate Professor Didier Talamona

April 2023

DECLARATION

I hereby, declare that this manuscript, entitled "*Powder Mixed EDM for biomedical alloys*", is the result of my own work except for quotations and citations, which have been duly acknowledged.

I also declare that, to the best of my knowledge and belief, it has not been previously or concurrently submitted, in whole or in part, for any other degree or diploma at Nazarbayev University or any other national or intentional institution.

Name: Nurlan Nauryz

Date: 14.04.2023

Abstract

The biomedical application of implants is currently becoming one of the most promising manufacturing methods. In fact, due to the challenging environment of the human body for biomedical implants, bio-implant manufacturing technologies should possess bio-functional characteristics on the surface. However, existing methods of implant manufacturing have some limitations, such as thin and nonuniform coating, and the inability to coat porous surfaces, which is possible with EDM. This review focuses on biomedical materials of implant that applies replacement of hard tissue in the human body. As it was found, Ti alloys with β stabilizers are the most biocompatible alternative for human bone replacement due to their unique advantages over other implant materials. On top of that, surface modification can be done by powder mixed-electro discharge machining (PMEDM). This technique allows for obtaining mechanical properties similar to the bone as well as increasing surface topology resulting in better biocompatibility.

This research aims to improve the biocompatibility of Ti-6Al-4V titanium alloy through Powder Mixed EDM machining. A systematic investigation was conducted on multi-scale EDM machines, resulting in significant improvements in machining performance by optimizing input parameters and powder additive concentration in dielectric. The results of macro and micro EDM experiments indicate that careful selection and optimization of parameters can enhance efficiency and quality. Furthermore, micro wire EDM machining can effectively reduce bacterial adhesion on metallic surfaces, making it a promising method for biomedical applications. The SEM and EDS results suggest that a proper combination of base material, electrode tool, dielectric, and powder additive can enhance biocompatibility. These findings have significant implications for biomedical applications of Ti-6Al-4V titanium alloy, and further studies can investigate the effectiveness of Powder Mixed EDM machining on other metallic materials and its potential applications in various biomedical fields.

Acknowledgements

I would like to express my deepest gratitude to my family for their unwavering support and encouragement throughout my academic journey. Their love and guidance have been instrumental in my success and have helped me to achieve my goals.

I am also grateful to my supervisor professor Asma Perveen and co-supervisor professor Didier Talamona for their invaluable guidance, mentorship, and support throughout this project. Their expertise, insight, and encouragement have been invaluable in helping me to achieve my research objectives.

I would also like to extend my sincere thanks to my colleague Salikh Omarov for his invaluable contribution to this project. His dedication, hard work, and our collaboration have been instrumental in achieving the goals of this research.

Furthermore, I would like to thank Professor Tri Pham, Ainur Kenessova, and Faisal Nazir from the Biological Department for their tremendous assistance and understanding during our research project.

Special thanks are owed to the committee member, Professor Yerkin Abdildin, for his insightful guidance and feedback on my Master's Thesis lectures, and for his valuable inputs during our personal rehearsals of the final presentation.

Finally, I would like to express my gratitude to all the faculty members of the Nazarbayev University School of Engineering and Digital Science (SEDS) for their support, encouragement, and guidance in nurturing future researchers in Kazakhstan.

Table of Contents

Abstract 2
Acknowledgements 3
Table of Contents 4
List of Abbreviations & Symbols 5
List of Tables 6
List of Figures 7
Chapter 1 – Introduction 8
1.1 Background 8
1.2 Problem Statement 8
1.3 Motivation 8
1.4 Aims and Objectives 9
Chapter 2 – Literature Review 10
2.1 Electrical Discharge Machining 10
2.2 Micro EDM 12
2.3 Powder Mixed EDM 15
2.3.1 PMEDM process 15
2.3.2 PMEDM process variables 16
Chapter 3 – Methodology 18
3.1 Ti-6Al-4V alloy 18
3.2 Powder (HA) 18
3.3 Experimental Study 19
3.3.1 Macro EDM 19
3.3.2 Micro EDM 20
3.3.3 Wire EDM 21
3.4 Post Characterization 22
3.4.1 Optical Microscope and Scanning Electron Microscope 22
3.4.2 Hardness testing 23
3.4.3 Surface roughness 23
3.4.4 Contact angle 24
3.4.5 Bacterial Attachment 25

Chapter 4 –Results 27
4.1 Macro EDM 27
4.1.1 MRR 27
4.1.2 Overcut 28
4.2 Micro EDM 31
4.2.1 MRR 32
4.2.2 Overcut 35
4.3 Optical microscope and SEM 37
4.4 Crater Size 39
4.5 Hardness test results 42
4.6 Surface roughness 44
4.7 Contact angle 45
4.8 Biological attachments 47
Chapter 5 – Conclusion 50
References 52
Appendix 55

List of Abbreviations & Symbols

EDM	Electro Discharge Machining
PMEDM	Powder Mixed Electro Discharge Machining
HA	Hydroxyapatite
MRR	Material removal rate

List of Tables

TABLE 1: THE PRIMARY DISCOVERIES OF RESEARCH FOCUSED ON THE SUBJECT OF EDM. 11
TABLE 2: MICRO-EDM SURFACE MODIFICATION RESULTS 14
TABLE 3: SUMMARY FOR DIFFERENT POWDER MATERIALS 16
TABLE 4: PMEDM FOR SURFACE MODIFICATIONS. 17
TABLE 5: CHEMICAL COMPOSITION OF TI-6AL-4V [39, 40]. 18
TABLE 6: EQUIPMENT SETUP FOR MACRO EDM. 19
TABLE 7: EXPERIMENTAL DESIGN FOR TI-6AL-4V ALLOY 20
TABLE 8: EXPERIMENTAL SCHEDULE 20
TABLE 9: RESPONSE TABLE FOR SIGNAL TO NOISE RATIOS FOR 0 GRAM PER LITER HYDROXYAPATITE POWDER CONCENTRATION 27
TABLE 10: RESPONSE TABLE FOR SIGNAL TO NOISE RATIOS FOR 5 GRAM PER LITER HYDROXYAPATITE POWDER CONCENTRATION 27
TABLE 11: RESPONSE TABLE FOR SIGNAL TO NOISE RATIOS FOR 0 GRAM PER LITER HYDROXYAPATITE POWDER CONCENTRATION 29
TABLE 12: RESPONSE TABLE FOR SIGNAL TO NOISE RATIOS FOR 5 GRAM PER LITER HYDROXYAPATITE POWDER CONCENTRATION 29
TABLE 13: MRR AND OVERCUT VALUES FOR DIFFERENT LEVELS OF CAPACITANCE, VOLTAGE, AND POWDER CONCENTRATION 31
TABLE 14: RESPONSE TABLE FOR SIGNAL TO NOISE RATIOS FOR MATERIAL REMOVAL RATE (MRR) VERSUS CAPACITANCE, VOLTAGE, AND POWDER CONCENTRATION 33
TABLE 15: ANALYSIS OF VARIANCE (ANOVA) TABLE FOR MRR VERSUS CAPACITANCE, VOLTAGE, AND POWDER CONCENTRATION 33
TABLE 16: RESPONSE TABLE FOR SIGNAL TO NOISE RATIOS FOR OVERCUT VERSUS CAPACITANCE, VOLTAGE, AND POWDER CONCENTRATION 35
TABLE 17: ANALYSIS OF VARIANCE (ANOVA) TABLE FOR OVERCUT VERSUS CAPACITANCE, VOLTAGE, AND POWDER CONCENTRATION 36
TABLE 18: ELEMENTAL ANALYSIS OF TI-6AL-4V PLATE AFTER MICRO-EDM TREATMENT 39
TABLE 19: CRATER AREA VALUES FOR DIFFERENT LEVELS OF CAPACITANCE, VOLTAGE, AND POWDER CONCENTRATION 40
TABLE 20: RESPONSE TABLE FOR SIGNAL TO NOISE RATIOS FOR OVERCUT VERSUS CAPACITANCE, VOLTAGE, AND POWDER CONCENTRATION 41
TABLE 21: HARDNESS VALUES FOR ALL EXPERIMENTS 42
TABLE 22: RESPONSE TABLE FOR SIGNAL TO NOISE RATIOS FOR SURFACE HARDNESS VALUES VERSUS CAPACITANCE, VOLTAGE, AND POWDER CONCENTRATION 43
TABLE 23: SURFACE ROUGHNESS MEASUREMENTS FOR MICRO WIRE EDM TREATED TI-6AL-4V WORKPIECES. 44
TABLE 24: SURFACE CONTACT ANGLE MEASUREMENTS FOR MICRO WIRE EDM TREATED TI-6AL-4V WORKPIECES. 46

List of Figures

FIGURE 1: BASIC PRINCIPLE OF EDM. 11
FIGURE 2: SURFACE LAYERS AFTER EDM TREATMENT. 11
FIGURE 3: MICRO EDM SCHEMATICS [14] 13
FIGURE 4: SCHEMATICS OF THE PMEDM PROCESS [23] 15
FIGURE 5: RESEARCH TREND FOR "HYDROXYAPATITE" & "PMEDM" IN GOOGLE SCHOLAR. 19
FIGURE 6: TI-6AL-4V MACHINE PLATES WITH MICRO WIRE EDM 22
FIGURE 7: CONTACT ANGLE MEASUREMENT FOR MICRO WIRE EDM MACHINED TI-6AL-4V PLATES 25
FIGURE 8: MEAN OF SN RATIOS FOR MRR VERSUS DISCHARGE CURRENT, TIME-ON, TIME-OFF, GAP VOLTAGE FOR 0 AND 5 G/L CONCENTRATION. 27
FIGURE 9: MEAN OF SN RATIOS FOR MRR VERSUS DISCHARGE CURRENT, TIME-ON, TIME-OFF, GAP VOLTAGE 29
FIGURE 10: MICROSCOPE PHOTOS OF THE THROUGH (LEFT) AND THE BLIND HOLES (RIGHT) OF TI-6AL-4V ALLOY BY USING MACRO EDM (MAGNIFICATION OF 5X) 31
FIGURE 11: MEAN OF SN RATIOS FOR MRR VERSUS CAPACITANCE, VOLTAGE, AND POWDER CONCENTRATION 32
FIGURE 12: MEAN OF SN RATIOS FOR OVERCUT VERSUS CAPACITANCE, VOLTAGE, AND POWDER CONCENTRATION. 35
FIGURE 13: OPTICAL MICROSCOPE CAPTURES OF MICRO-EDM TREATED TI-6AL-4V HOLES USING TUNGSTEN CARBIDE ELECTRODE TOOL FOR DIFFERENT DISCHARGE ENERGIES; (A) 100PF, 90V, (B) 100PF, 100V, (C) 100 PF, 110V, (D) 1NF, 90V, (E) 1NF, 100V, (F) 1NF, 110V, (G) 10NF, 90V, (H) 10NF, 100V, (I) 10NF, 110V AT CONSTANT ELECTRODE ROTATIONAL SPEED OF 1000 RPM. 37
FIGURE 14: SEM CAPTURES FOR DIFFERENT DISCHARGE ENERGIES FOR MICRO-EDM OF TI-6AL-4V USING TUNGSTEN CARBIDE ELECTRODE TOOL; (A) 100PF, 90V, (B) 100PF, 100V, (C) 100 PF, 110V, (D) 1NF, 90V, (E) 1NF, 100V, (F) 1NF, 110V, (G) 10NF, 90V, (H) 10NF, 100V, (I) 10NF, 110V AT CONSTANT ELECTRODE ROTATIONAL SPEED OF 1000 RPM. 38
FIGURE 15: MEAN OF SN RATIOS FOR CRATER AREA VALUES VERSUS CAPACITANCE, VOLTAGE, AND POWDER CONCENTRATION 41
FIGURE 16: MEAN OF SN RATIOS FOR SURFACE HARDNESS VALUES VERSUS CAPACITANCE, VOLTAGE, AND POWDER CONCENTRATION 43
FIGURE 17: CRYSTAL VIOLET STAINED AND BRIGHTFIELD PICTURES OF STAPHYLOCOCCUS AUREUS BACTERIAL ATTACHMENT ON MACHINED TI-6AL-4V ALLOY WITH LOW ENERGY (100PF, 90 V) FOR LEFT AND RIGHT CUTS. 47
FIGURE 18: CRYSTAL VIOLET STAINED AND BRIGHTFIELD PICTURES OF STAPHYLOCOCCUS AUREUS BACTERIAL ATTACHMENT ON MACHINED TI-6AL-4V ALLOY WITH MEDIUM ENERGY (1NF, 100 V) FOR LEFT AND RIGHT CUTS. 47
FIGURE 19: CRYSTAL VIOLET STAINED AND BRIGHTFIELD PICTURES OF STAPHYLOCOCCUS AUREUS BACTERIAL ATTACHMENT ON MACHINED TI-6AL-4V ALLOY WITH HIGH ENERGY (10 NF, 110 V) FOR LEFT AND RIGHT CUTS. 48
FIGURE 20: CRYSTAL VIOLET STAINED AND BRIGHTFIELD PICTURES OF ESCHERICHIA COLI BACTERIAL ATTACHMENT ON MACHINED TI-6AL-4V ALLOY WITH LOW ENERGY (100PF, 90 V) FOR LEFT AND RIGHT CUTS. 48
FIGURE 21: CRYSTAL VIOLET STAINED AND BRIGHTFIELD PICTURES OF ESCHERICHIA COLI BACTERIAL ATTACHMENT ON MACHINED TI-6AL-4V ALLOY WITH MEDIUM ENERGY (1NF, 100 V) FOR LEFT AND RIGHT CUTS. 48
FIGURE 22: CRYSTAL VIOLET STAINED AND BRIGHTFIELD PICTURES OF ESCHERICHIA COLI BACTERIAL ATTACHMENT ON MACHINED TI-6AL-4V ALLOY WITH HIGH ENERGY (10NF, 110 V) FOR LEFT AND RIGHT CUTS. 48

Chapter 1 – Introduction

1.1 Background

Metal biomedical alloys, which are primarily used as bio-implant material, are implanted into the body to repair broken bones and degenerated joints caused by unexpected injury and aging. The phrase "biomaterials" pertains to deliberately designed materials, whether they are artificial or organic, that have the potential to extend an individual's lifespan and augment their standard of living. These substances are intended to replace or restore damaged, absent, or diseased human body parts such as bones, teeth, ligaments, and the heart. The application of these bio-implants encompasses a range of medical areas, including orthopedics, dentistry, cardiology, and vascular surgery. Orthopedic implants, dental implants, heart valves, artificial hearts, and vascular grafts are among the most widely used biomaterials in the field of regenerative medicine, as they are capable of reconstituting damaged tissues and organs. The tremendous rise in the elderly in the world has led to a huge growth in the use of biomaterials and has attracted researchers' interest to it [1].

1.2 Problem Statement

Almost 80% of metallic biocompatible alloys, which are used in bio-implant manufacturing, are materials that possess high tensile strength, durability, and fracture toughness. Titanium, cobalt-chromium, and amorphous alloys are the commonly utilized metals in the bio-implant's industry [2]. Due to their artificial construction and potential complications after implantation, these implants have a limited bio-functional response. The release of toxic ions and particles into the tissues nearby, which promotes cell inflammation and adverse reactions in the host tissues, is one of the biggest problems. Another issue is a physiological response that causes isolation between the implants and bone as a result of the formation of a fibrous capsule. Additionally, the high elasticity modulus of these biomaterials shielded the bone from stress, resulting in bone resorption and implant loosening after implantation [3].

1.3 Motivation

Overall, there are existing techniques to overcome the abovementioned problems, such as chemical vapor deposition, plasma spraying, sol-gel, physical vapor deposition, dip coating and etc. Moreover, they have already found their use in bio-implant manufacturing.

However, as most of the techniques are known for a lengthy time, these techniques also have some drawbacks to improve. They cannot generate flawless, porous surfaces and cannot deposit coating and shape specimens concurrently, resulting in an increased processing cost, which in turn is possible with EDM [4].

1.4 Aims and Objectives

The aim of this project is to develop a thorough understanding of the Powder Mixed EDM machining performance on Ti-6Al-4V, by undertaking a systematic investigation on multi-scale EDM processes in order to improve surface biocompatibility. Following is the list of objectives that are set to accomplish the principal aim of the research:

1. To examine the macro-EDM machining performance with and without the addition of the hydroxyapatite powder into the dielectric fluid forTi-6Al-4V.
2. To examine the micro-EDM machining performance with and without the addition of hydroxyapatite powder into the dielectric fluid.
3. To study the surface characteristics parameters, such as surface roughness, hardness, and crater size after Powder Mixed EDM treatment.
4. To examine the bacterial attachment and adhesion after PM wire EDM treatment.

Chapter 2 – Literature Review

2.1 Electrical Discharge Machining

EDM is a machining method that has several advantages over traditional methods, including the ability to manufacture hard-to-machine materials with high precision and a excellent surface finish [5]. It works by using sparks between a conductive workpiece and an electrode tool, which prevents mechanical deformation [5]. There are several variations of EDM, such as dry EDM, die-sinking EDM, wire EDM, micro-EDM, and powder-micro-EDM, each with different material removal rates and discharge energy values [5].

The Electrical Discharge Machining (EDM) technique converts electrical energy into thermal energy by creating a sequence of electrical discharges between the workpiece and the electrode in the presence of a dielectric fluid [6]. Process schematics can be seen from figure 1. These discharge sparks lead to a formation of a crater on the workpiece surface, which causes an alteration in the metal zone, known as the Altered Metal Zone (AMZ). The AMZ consists of three layers, namely, the spattered surface layer, the recast layer, and the heat-affected zone (HAZ). [6]. The spattered surface layer is the topmost layer, and it comprises debris that has been ejected from the workpiece surface due to the force generated by the discharge sparks. The recast layer is the middle layer, which has undergone a melting and solidification process, resulting in a new solid layer. The HAZ is the deepest layer, and it experiences heat exposure that alters its mechanical and metallurgical properties. The three-layer structure of the AMZ plays a significant role in determining the quality and precision of the EDM process, making it a vital area of study in the field of materials engineering [6]. Illustration for the HAZ can be found in figure 2. Table 1 shows some key findings.

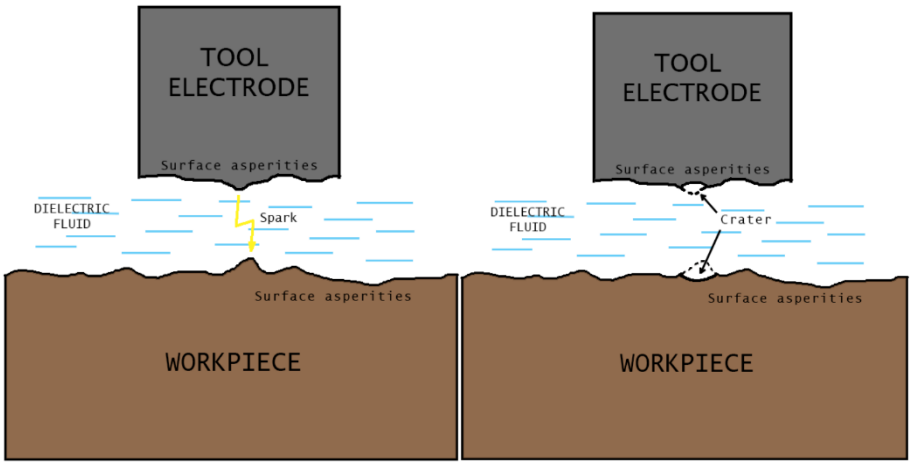

Figure 1: Basic principle of EDM.

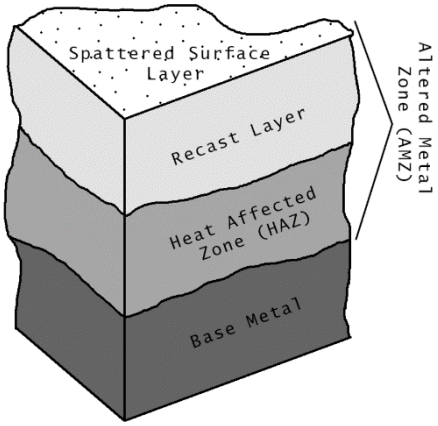

Figure 2: Surface layers after EDM treatment.

Table 1: The primary discoveries of research focused on the subject of EDM.

Authors	Key findings
Tanjilul *et al.* [7]	• Developed an innovative debris removal method that improves deep-hole EDM drilling efficiency. • Decrease in the duration required for drilling and enhancement of the surface texture.
Abu *et al.* [8]	• Provided a comprehensive review of EDM research on titanium and its alloys. • Summarized practical and theoretical investigations to enhance process efficiency. • Evaluated MRR, tool wear, surface roughness, and other response

	variables.
Kumar *et al*. [9]	• Multiple approaches have been suggested to boost the efficacy of the Electrical Discharge Machining (EDM), including incorporating a cryogenically cooled electrode or introducing a magnetic field to the sparking area. • Found that by selecting ideal process parameter combinations, they achieved the highest achievable Material Removal Rate (MRR) attained was 47 milligrams per minute, and the least possible Surface Roughness (SR) was 1.487 micrometers, representing a 44% and 51% increase, respectively, in comparison to the conventional EDM technique.
Muthuramalingam & Mohan [10]	• Analyzed multiple input variables for modeling and their effects, such as the pulse width and the electrode's shape. • Discussed the effect of discharge energy on MRR, surface roughness, and electrode wear rate. • Explored how to control electrical process parameters and optimize process parameters.
Chakraborty *et al.* [11]	• Conducted a literature review on the utilization of dielectric fluids in EDM. • The use of high pulse energy resulted in a higher Material Removal Rate (MRR) and reduced wear when operating in distilled water, as compared to machining in kerosene. • It was shown that gaseous dielectrics like air and oxygen can also be used for EDM and may remove more material at a faster rate than hydrocarbon oil. • The suggestion was made that the use of dielectric fluids with low viscosity can enhance the micro-effectiveness of Electrical Discharge Machining (EDM), whereas hydrocarbon-based lubricants have minimal influence on the machining cycle time

2.2 Micro EDM

The non-conventional Micro-electrical discharge machining (Micro-EDM) has become an effective technique in the micro-component processing industry due to its non-contact approach, capable of machining different types of materials with minimal force. Micro-EDM can produce high-quality and precise machining with appropriate parameters. It is suitable for hard die materials and surface modification for localized coating of microscopic components [12]. However, the method has limitations such as low MRR and high tool wear, which can be mitigated by electrode wear adjustment or elongation. Micro-EDM operates on similar principles

to conventional EDM, but with smaller tool size and lower discharge energy. Figure 3 shows the process schematics.

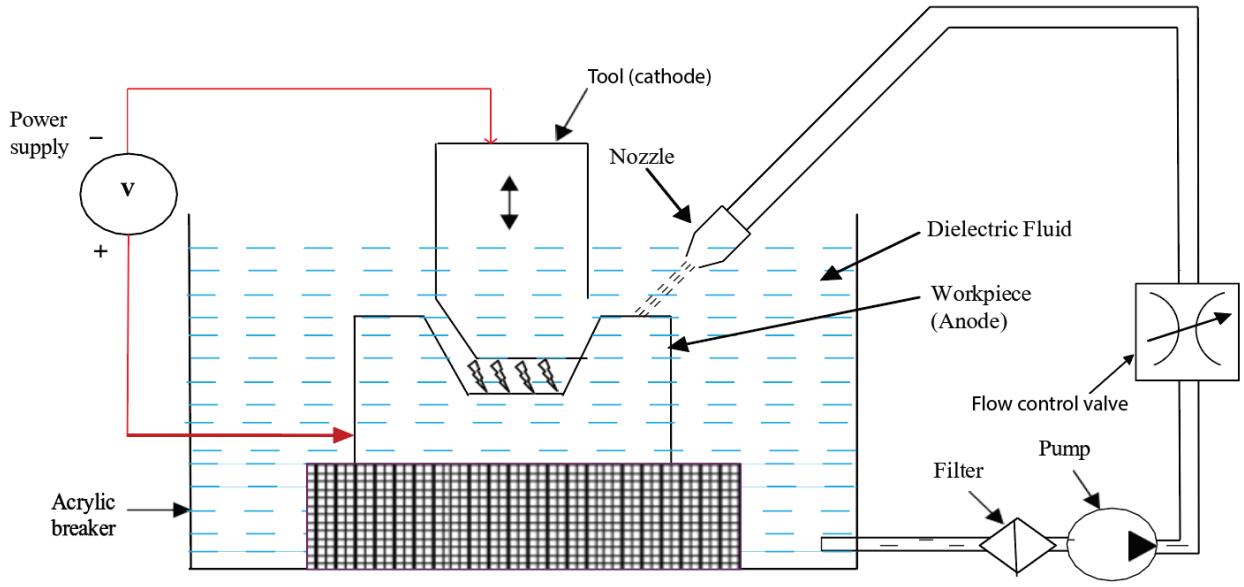

Figure 3: Micro EDM schematics [13]

Surface modification research shows promising results for the method, including solid-lubricating coating and intermetallic compound formation on the surface of a Ti6Al4V workpiece. Mixing conductive powder into the dielectric fluid is another updated Micro-EDM technique that widens spark gaps and improves surface quality.

The main criteria for the machine to be able to operate at the microscale are extremely accurate machinery and a small material removal unit [14]. A tiny unit removal criterion in the context of micro-EDM typically indicates that the discharge energy (W_e) created in the sparking gap during one pulse must be as low as feasible, which can be achieved with the use of criteria relaxation capacitance type of power generator.

$$W_e = \int_0^{te} u_e(t) i_e(t) dt \tag{1}$$

Here, u_e is voltage across the gap, i_e is the currents, and t is the pulse-on duration.

The conventional EDM method, which employs a static iso-energetic pulse generator to turn on/off DC power using a transistor, poses a challenge in delivering short pulse duration

times because of the long delay time for the discharge current to fall to zero after detecting a discharge. To address this issue, micro-EDM generators based on resistance-capacitance (RC) technology are frequently used to create pulses, which can significantly reduce the pulse duration by using modest capacitance and lowering the inductance of the discharge circuit [15].

According to Kieswetter *et al.* and Buser *et al.*, The microstructure of a material is significantly affected by its surface, which can also have a profound impact on the cells surrounding biomedical implants, resulting in an accelerated development of bone or tissue. [16, 17]. To examine the surface characteristics of biomedical alloys, including NiTi shape-memory alloy and high-strength Ti-6Al-4V, Jahan *et al.* employed micro-EDM. The microstructure of the machined surface revealed a modification in topography due to microhardness. NiTi displayed an average hardness of 420.9 HV before machining, which rose to 524.4 HV post-machining. Ti-6Al-4V, on the other hand, had an average hardness of 429.5 HV prior to machining and 481.6 HV following machining. [18]. Table 2 provides literature evidence of the impact of micro-EDM on material surfaces.

Table 2: Micro-EDM surface modification results

Authors	Outcomes
Jahan *et al.* [19]	• Studied the possibility of enhancing the surface properties of carbide with micro-EDM milling with the addition of graphite nano powder to the dielectric. Achieved a defect-free and smooth surface.
Kiran *et al.* [20]	• Demonstrated that the utilization of micro-EDM dielectric leads to a reduction in thickness layer. • Found that the micro hardness of Ti6Al4V treated with micro-EDM using standard EDM oil was between 286.81 and 495.9 HV. Observed that the average surface roughness value of the samples decreased when powder materials were added to the dielectric.
Wang *et al.* [21]	• The study showed that an increase in electrode size caused an increase in surface roughness values. The use of deionized water as a dielectric instead of EDM oil resulted in a reduction of surface roughness due to its lower viscosity. Additionally, the amount of surface defects, such as micro-voids and micro-cracks, decreased as the discharge energy decreased.

2.3 Powder Mixed EDM

2.3.1 PMEDM process

Powder mixed electrical discharge machining (PMEDM) is an innovative application of EDM technology that utilizes metallic powder materials in the dielectric fluid to enhance performance and surface finish. By adding these materials, the insulating strength of the fluid is reduced, resulting in a wider inter-electrode gap. Powder Mixed Electric Discharge Machining (PMEDM) operates by applying a voltage between positive and negative charges of metallic powder materials, which generates an electric field. As the particles become energized, they move in a zigzag pattern, increasing the inter-electrode gap and leading to a superior surface finish. PMEDM has been shown to be more effective than conventional EDM. A schematic of the PMEDM process can be seen in Figure 4 [22].

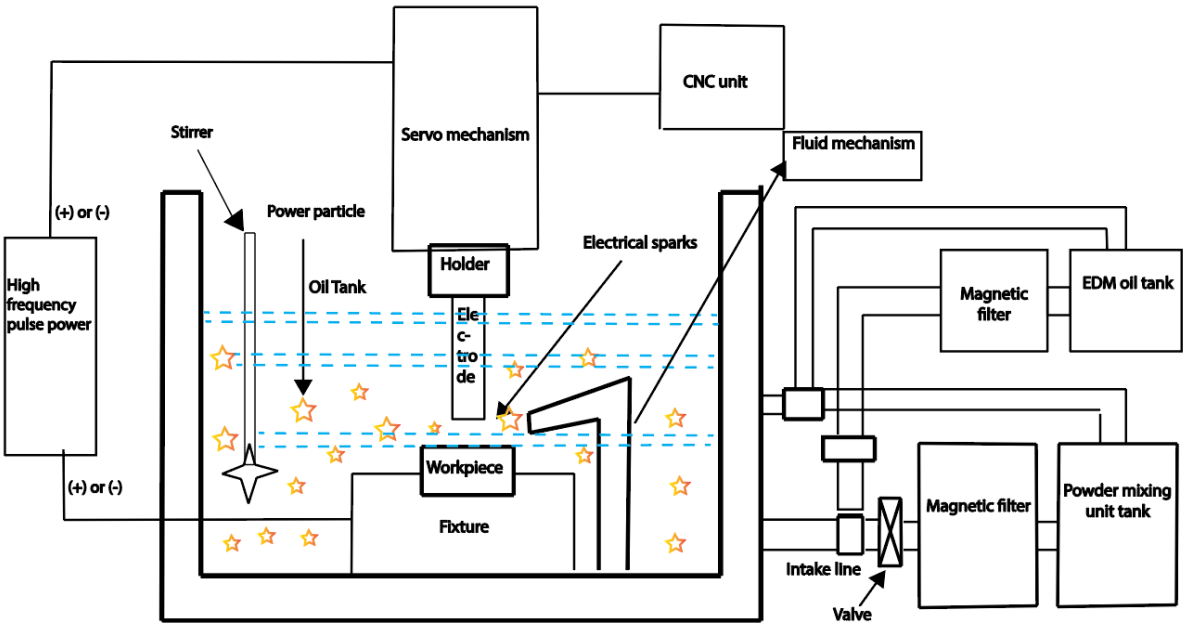

Figure 4: Schematics of the PMEDM process [23]

The combination of powder particles with the dielectric in EDM can increase the discharge gap. This increase in discharge gap is influenced by the electrical and physical properties of the powder particles. At high temperatures, powder particles can decrease the dielectric resistance and initiate sparks that travel longer distances. Once a spark occurs, the energized powder particles move with the ions and electrons, producing more electric charges,

and reducing the hydrostatic pressure in the plasma channel, ultimately leading to an increased discharge gap. The larger shallow cavities created through this process increase the material removal rate and improve the surface finish, while also reducing the number and size of micro-cracks. In addition, the incorporation of powder into the dielectric fluid can promote biocompatibility by enhancing the properties of cell adhesion and proliferation. [24-26].

2.3.2 PMEDM process variables

Various process variables impact the Powder Mixed EDM machining's performance and are classified into four groups: electrical, powder, non-electrical, and electrode-based parameters [27]. The electrical parameters consist of several variables such as peak current, discharge voltage, pulse-on and pulse-off times, duty cycle, polarity, electrode gap, and gap voltage. Adjusting these parameters can modify machining performance, such as material removal rate, surface roughness, and tool wear rate.

Non-electrical parameters also contribute to machining performance. Dielectric flushing ensures machining accuracy and removes debris from the workpiece. Workpiece and electrode rotation improves surface roughness and inter-electrode flushing, respectively. Dielectric fluid, the third type of non-electrical parameter, serves as an insulating medium, removes debris, and dissipates heat from the electrode tool.

The powder material is another parameter that enhances machining performance. Table 3 presents a brief summary of each powder material type.

Table 3: Summary for different powder materials

Powder material	Primary outcomes
Aluminum (Al)	Desire final shape, reduction in TWR, excellent surface finish[28]
Silicon Carbide (SiC)	Increase in Surface roughness, MRR and TWR [29]
Chromium (Cr)	Improvement in machining efficiency, reduction in TWR
Silicon (Si)	Reduction in surface roughness [30], [31]
Titanium (Ti)	Surface hardness increase, fewer occurrences of micro-cracks were observed [32]
Tungsten (W)	Surface micro hardness increase, part life increase
Boron Carbide	Improvement in machining efficiency and MRR [33]

(B4C)	
Graphite (Gr/C)	Increase in electrical conductivity, improvement in MRR and reduction in TWR [34]
Molybdenum (Mo)	Tensile strength and conductivity increase [35]
Alumina (Al2O3)	Improvement in topography and surface finish [35]
Carbon nanotubes (CNTs)	Reduction in surface roughness, surface crack's size and recast layer thickness [35]

In Powder Mixed Electric Discharge Machining (PMEDM), the electrode tool plays a crucial role, and its effectiveness is usually assessed based on three primary output characteristics: MRR, electrode tool wear rate, and final surface roughness. The material and shape of the electrode have the most significant impact on its performance [36]. Table 4 illustrates the literature conducted on the surface modifications for the PMEDM.

Table 4: PMEDM for surface modifications.

Authors	Powder	Outcomes
Y. Lamichhane [37]	Hydroxyapatite (HA)	• Enhancement in surface texture with an increase in current parameter. Reduced number of voids, cracks, and craters due to the addition of HA powder according to SEM results. • XRD analysis showed the formation of several intermetallic compounds on the surface of 316L SS.
G. Sharma *et al.* [38]	Mg and Zr	• Better MRR and lower surface roughness values for Zr powder in comparison to Mg powder. • 40.74% reduction in corrosion rate for Mg-4Zn with Zr powder in comparison to unpolished surface.

Chapter 3 – Methodology

3.1 Ti-6Al-4V alloy

After evaluating several options, the beta alloy Ti-6Al-4V was chosen as a research material due to its lower elastic modulus and good fatigue properties when in a solution-treated state [39]. Table 5 shows the chemical composition of this alloy. Samples of this material were cut into pieces with dimensions of 20 mm × 20 mm with grinding method. Carbon steel and nickel alloy workpieces were used for the parameter optimization process of macro and micro EDM.

Table 5: Chemical composition of Ti-6Al-4V [39, 40].

Elements	Ti (wt.%)	Al (wt.%)	V (wt.%)	O (wt.%)	N (wt.%)
Weight percentage (%)	90	6	4	0.2	0.05

3.2 Powder (HA)

In addition to the powder materials mentioned earlier, Hydroxyapatite (HA) is a highly innovative and promising powder additive used in the industry. This molecule is recognized for its durability and crystal structure, which resembles that of the human skeleton, making it ideal for bone implants. Furthermore, it has superior biocompatibility and osseointegration than other powder additives, as well as a reduced risk of flammability and adverse chemical reactions. However, its load-bearing capacity is a significant constraint that can be resolved by blending it with other powders. The chemical composition of hydroxyapatite powder is Ca10(PO4)6(OH)2, which is a calcium phosphate mineral with the chemical formula Ca5(PO4)3(OH), but often contains other elements such as carbonate, fluoride, and chloride as impurities [41].

Numerous studies have examined the use of HA as an additive material for EDM, and three parameters - contact angle, structure pattern, and surface roughness - influence the biocompatibility of the implant, as they enable biomolecules to attach to the implant surface. Multiple experiments have demonstrated that HA has a positive impact on all three of these parameters. Furthermore, the growing research interest in HA powder over the last decade, as depicted in Figure 5, has made it a popular option as a powder material for various research projects.

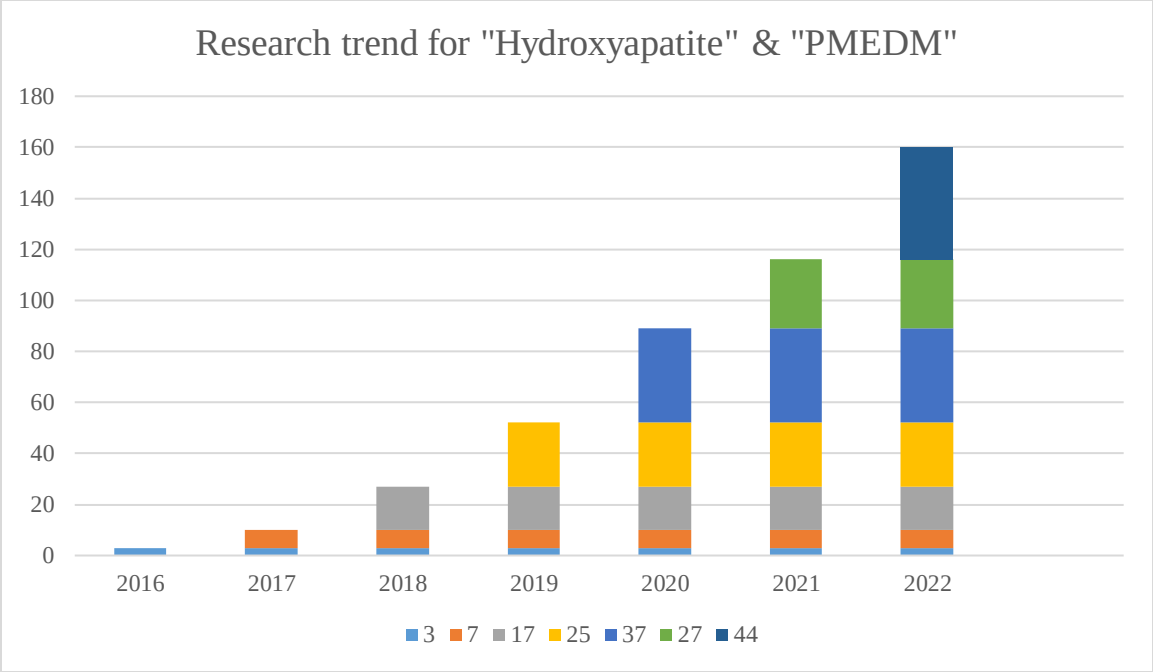

Figure 5: Research trend for "Hydroxyapatite" & "PMEDM" in google scholar.

3.3 Experimental Study

3.3.1 Macro EDM

In the next step, experiments on the macro EDM were conducted on Ti-6Al-4V alloy workpieces. Overall, 56 tests were performed by changing the parameters, such as working current (I), time-on, time-off, pulse current (C), servo speed and gap voltage. The tables for experiments conducted can be found in the appendix section. Each parameter was changed consequently in order to observe the effect of it on MRR and overcut. Moreover, the table for the equipment setup is listed in table 6.

Table 6: Equipment setup for Macro EDM

Equipment setup	Description
Machine	Drilling EDM DD703.30A
Tool electrode	Tubular brass electrode
Workpiece	Ti-6Al-4V alloy
Polarity	Tool (+), Workpiece (-)
Dielectric	Deionized water

Based on the data obtained from experimental sets of other materials, the orthogonal array for Ti-6Al-4V trials was created with 4 parameters in 3 dimensions. They are Pulse Current

(2, 5, 8), Time-on (2, 5, 8), Time-off (2, 5, 8) and Gap voltage (3, 6, 9). It can be seen from table 7. This experimental set up was repeated with addition of 5 gram per liter hydroxyapatite powder.

Table 7: Experimental design for Ti-6Al-4V alloy

No. exp.	Discharge current	Time-on	Time-off	Gap voltage
1	2	2	2	2
2	2	5	5	5
3	2	8	8	8
4	5	2	5	8
5	5	5	8	2
6	5	8	2	5
7	8	2	8	5
8	8	5	2	8
9	8	8	5	2

3.3.2 Micro EDM

The goal was to determine the best machining settings for titanium alloy on micro-EDM. Every experiment was compared by its discharge energy. The following formula describes how the system's capacitance and voltage affect the micro-discharge EDM's power:

$$E = \frac{CU^2}{2} \tag{2}$$

Capacitance and voltage settings were divided into 3 levels each, which are 100 pF (1), 1 nF (2), 10 nF (3), and 90 V, 100 V, and 110 V respectively.

Every experimental trial was conducted by using a 0.03 mm/min feed and the aim was to machine 0.050 mm in depth. Sets of 9 experiments were repeated for 0, 5 and 10 gram/liter powder concentrations. The table 8 lists the experimental schedule.

Table 8: Experimental schedule

Capacitance	Voltage	Powder concentration
3	90	0
3	90	0
3	90	0
3	100	5
3	100	5
3	100	5
3	110	10

3	110	10
3	110	10
4	90	5
4	90	5
4	90	5
4	100	10
4	100	10
4	100	10
4	110	0
4	110	0
4	110	0
5	90	10
5	90	10
5	90	10
5	100	0
5	100	0
5	100	0
5	110	5
5	110	5
5	110	5

3.3.3 Wire EDM

The current study employed wire electrical discharge machining (WEDM) methodology to investigate the effect of input parameters on the machining performance of Ti-6Al-4V titanium plates. Eighteen experiments were conducted, using 50-µm diameter tungsten wire to cut 3x20x0.025 mm dimensions on both sides of 9 titanium plates with dimensions of 20x20x3mm. as illustrated in figure 6.

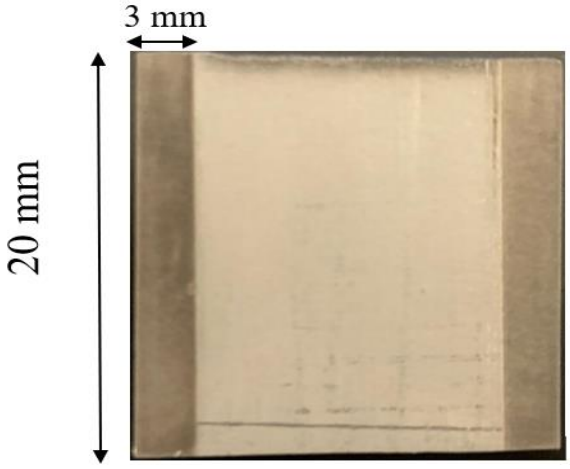

Figure 6: Ti-6Al-4V machine plates with micro wire EDM

Given the extensive time required for each experiment (3-4 hours), the number of input parameters was reduced by dividing them into three discharge energy values: low (100 pF and 90 V), medium (1 nF and 100 V), and high (10 nF and 110 V). Each discharge energy value experiment was then repeated for two sides of the titanium plate. Furthermore, to explore the impact of hydroxyapatite powder concentration, the entire process was repeated for 0, 5, and 10 gram per liter powder concentrations, resulting in a total of six experiments for each powder concentration. The chosen approach enabled the identification of optimal input parameters for wire EDM machining of Ti-6Al-4V plates, while also minimizing the number of experiments required.

3.4 Post Characterization

3.4.1 Optical Microscope and Scanning Electron Microscope

In this study, the Moticam 5+ optical microscope was employed to measure the diameter of the machined hole. This measurement was then used to estimate both the material removal rate and overcut values, which are essential parameters in evaluating the efficiency and accuracy of the wire EDM process. They are calculated according to the following formulas:

$$MRR = \frac{Area\ of\ the\ hole\ *\ depth}{Machining\ time} = \frac{\frac{\pi(D)^2}{4} * h}{t} \quad (3)$$

$$Overcut = \frac{Hole\ diameter\ at\ the\ entrance\ -\ electrode\ diameter}{2}$$

(4)

, where D is the diameter of the hole, h is the depth of cutting.

To investigate deeper into the surface features and structure of the machined samples, scanning electron microscopy (SEM) was employed. Specifically, the SEM was used to measure the discharge crater sizes and to observe the surface composition of the samples using energy dispersive X-ray spectroscopy (EDS). All discharge values were photographed in 10-µm scale to facilitate the visualization of differences in crater sizes. The obtained images were then analyzed using Imagej software to determine the precise sizes of the craters. Overall, the combined use of optical microscopy and SEM provided valuable insights into the material removal and surface characteristics of the machined samples, which are important in improving the performance of the wire EDM process.

3.4.2 Hardness testing

The present study employed the Falcon 300 hardness tester to investigate the hardness of machined samples. Specifically, the Vickers 200 g with a 10-second dwelling time was employed to acquire the hardness values. To ensure a comprehensive statistical dataset, three measurements were conducted for each of the 27 experiments performed via micro-EDM. The hardness values were then analyzed and compared to evaluate the effect of different input parameters on the hardness of the samples. The Falcon 300 hardness tester is a widely used tool in the field of materials science and provides accurate and reliable results, making it an ideal choice for measuring the hardness of the machined samples in this study. The use of this methodology allowed for a thorough investigation of the relationship between the input parameters and the resulting hardness values, which can aid in optimizing the micro-EDM process for improved efficiency and precision.

3.4.3 Surface roughness

In this study, surface roughness measurements were conducted on Ti-6Al-4V plates that were machined by micro wire EDM. A Portable Surface Roughness Gauge was utilized for the purpose of these measurements. A total of 18 experiments were conducted, with 3 experiments conducted for each combination of micro wire EDM input parameters. The experiments were designed to investigate the effects of micro wire EDM input parameters on surface roughness.

Prior to conducting the surface roughness measurements, the height of the probe position was calibrated using the built-in levelling indicator of the Portable Surface Roughness Gauge. This ensured that accurate and consistent measurements were taken throughout the course of the experiments.

During each experiment, measurements were taken on both sides of the Ti-6Al-4V plates. This approach was adopted to ensure that both sides of the plate were equally analyzed and accounted for in the final results. The Portable Surface Roughness Gauge was positioned at a fixed angle relative to the surface being measured, with the probe being moved along the surface to record the surface roughness measurements.

3.4.4 Contact angle

The contact angle measurements of Ti-6Al-4V plates were conducted utilizing The OCA 25 contact angle measurement machine, in this study. Micro wire EDM was utilized to machine the Ti-6Al-4V plates, and three experiments were performed for each combination of micro wire EDM input parameters. A total of 18 experiments were performed in this study, with deionized water utilized as the liquid for contact angle measurements.

The contact angle measurement in this study was conducted using the sessile drop method, which is a well-known and widely used technique. In this method, a droplet of liquid is placed on a solid surface, and the angle between the liquid and the surface is measured. Deionized water was chosen as the liquid in this study due to its low surface tension and excellent wettability properties.

The in-built calculator present in the software was utilized to estimate the contact angle values and was employed to ensure that the contact angle values obtained were accurate and reliable as in figure 7.

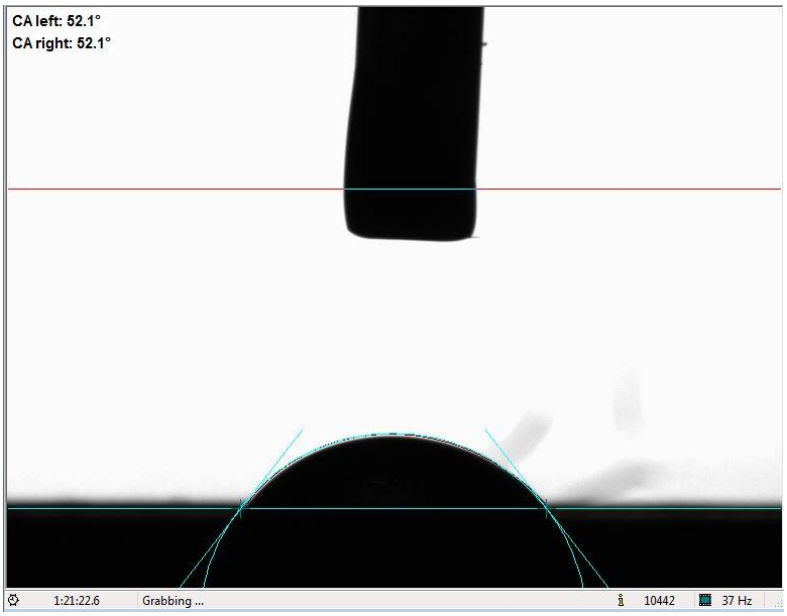

Figure 7: Contact angle measurement for micro wire EDM machined Ti-6Al-4V plates

3.4.5 Bacterial Attachment

The present study aimed to investigate the antibacterial efficacy of Ti-6Al-4V against various bacterial strains, namely Staphylococcus aureus and Escherichia coli DH5-Alpha, by quantifying biofilm formation on different metal surfaces after 48 hours of inoculation in broth culture. To prepare the bacterial inoculum, a fresh 24-hour liquid culture of each bacterial species was used to obtain an initial optical density (OD 600) of 0.1 or McFarland turbidity of 0.5. The OD 600 of the 24-hour culture broth was measured using a plate reader, and the required volume of bacteria was calculated using the standard formula $C_1V_1 = C_2V_2$, where C_1 and C_2 are the initial and final OD values, and V_1 and V_2 are the initial and final volumes. The required amount of bacteria was added to a fresh medium in a 50 mL Falcon tube to form a final volume of 50 mL with an OD of 0.1.

Each metal alloy piece was suspended in a separate 50 mL Falcon tube containing a single bacterial species in the culture medium. These tubes were incubated under aerobic conditions in a shaker incubator at 37°C and a speed of 220 RPM for 48 hours. To detect bacterial cells and biofilm formation on the metal surfaces, the samples were stained with crystal violet dye by dipping them in the solution for 30 minutes. The stained samples were rinsed three times with distilled water and air-dried at room temperature for 1 hour before imaging. The

samples were observed and imaged using the Zeiss AxioZoom V16 microscope, with images taken using both brightfield and a red fluorescent emission filter set.

Biofilm coverage quantification was done using custom written MatLab code. To ensure the cleanliness and sterilization of the metals between experiments, they were first immersed in a 30% acetic acid solution for 15 minutes to remove any biofilms on the surfaces, then washed with water, and finally dipped into a 70% ethanol solution for 30 minutes and plasma cleaned for 5 minutes. Before each biofilm formation test, all metals were sterilized under UV light for 30 minutes.

It is worth noting that S. aureus was grown in tryptic soy medium (TSB), while P. aeruginosa and E. coli DH5-Alpha were grown in Luria-Bertani (LB) broth. This methodology was conducted under aseptic conditions to maintain the integrity of the experimental results.

Chapter 4 –Results

4.1 Macro EDM

4.1.1 MRR

After conducting experiments, the effect of each machining parameter was analyzed and illustrated in relation to the MRR in the following figures:

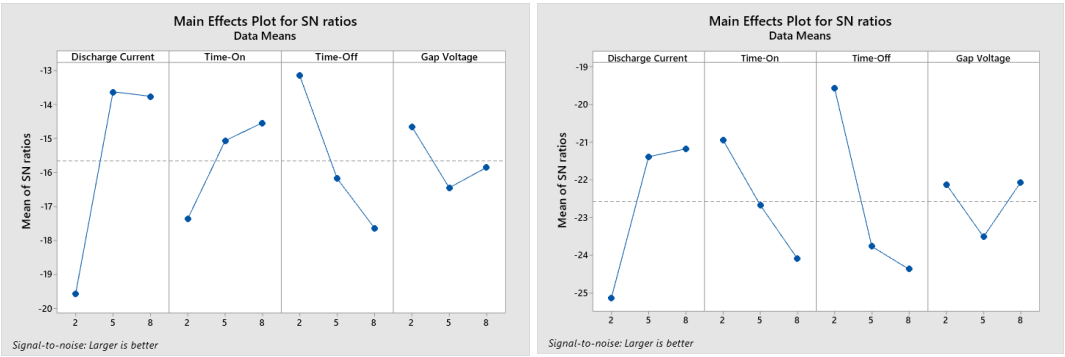

Figure 8: Mean of SN ratios for MRR versus Discharge current, Time-on, Time-off, Gap voltage for 0 and 5 g/l concentration.

Table 9: Response Table for Signal to Noise Ratios for 0 gram per liter hydroxyapatite powder concentration

Level	Discharge current	Time-On	Time-Off	Gap voltage
1	-19.58	-17.36	-13.15	-14.66
2	-13.63	-15.07	-16.18	-16.46
3	-13.76	-14.54	-17.65	-15.86
Delta	5.95	2.82	4.5	1.79
Rank	1	3	2	4

Table 10: Response Table for Signal to Noise Ratios for 5 gram per liter hydroxyapatite powder concentration

Level	Discharge current	Time-On	Time-Off	Gap voltage
1	-25.14	-20.95	-19.57	-22.13
2	-21.39	-22.67	-23.77	-23.52
3	-21.18	-24.09	-24.38	-22.07
Delta	3.96	3.14	4.81	1.44
Rank	2	3	1	4

Table 9 displays the results for MRR versus Discharge Current, Time-On, Time-Off, and Gap Voltage with a concentration of 0 grams per liter of hydroxyapatite powder. The highest signal-to-noise ratio was achieved at level 1 for Discharge Current, with a value of -19.58, while level 1 also had the highest signal-to-noise ratio for Time-On, with a value of -17.36. Additionally, level 1 had the highest signal-to-noise ratio for Time-Off, with a value of -13.15, and for Gap Voltage, with a value of -14.66. SN ratios here are used to maximize the MRR.

In contrast, Table 10 displays the results for MRR versus Discharge Current, Time-On, Time-Off, and Gap Voltage with a concentration of 10 grams per liter of hydroxyapatite powder. Here, the highest signal-to-noise ratio was achieved at level 1 for Time-Off, with a value of -19.57, while level 2 had the highest signal-to-noise ratio for Time-On, with a value of -22.67. Furthermore, for Discharge Current, level 1 had the second-highest signal-to-noise ratio, with a value of -25.14, and for Gap Voltage, level 1 had the lowest signal-to-noise ratio, with a value of -22.13.

Analyzing both tables, it is apparent that the highest signal-to-noise ratios are generally greater in Table 10 than in Table 9, indicating that increasing the concentration of hydroxyapatite powder may have a positive effect on the MRR. Furthermore, the rank order of the levels for each factor differs in the two tables, which suggests that the optimal settings for each factor may vary depending on the concentration of hydroxyapatite powder. These findings can be utilized to enhance the MRR process by identifying the optimal settings that lead to the highest signal-to-noise ratios for each factor at different concentrations of hydroxyapatite powder.

4.1.2 Overcut

After conducting experiments, the effect of each machining parameter was analyzed and illustrated in relation to the Overcut in the following figures:

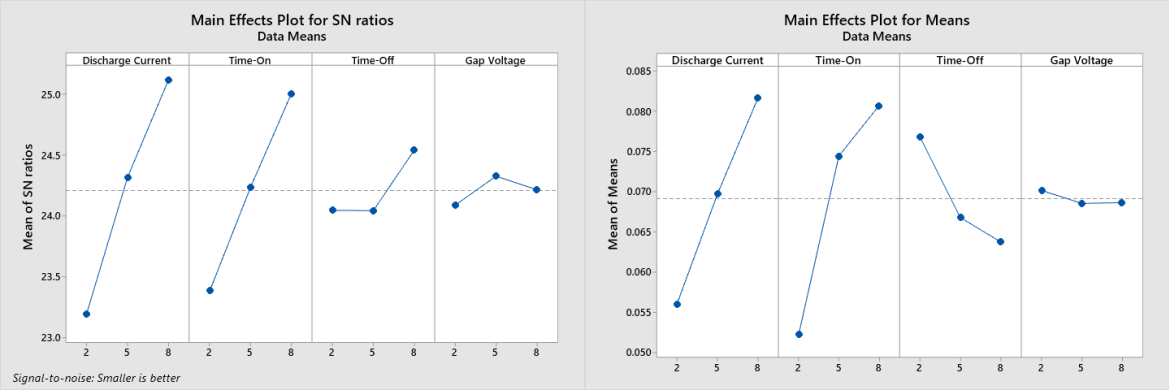

Figure 9: Mean of SN ratios for Overcut versus Discharge current, Time-on, Time-off, Gap voltage

Table 11: Response Table for Signal to Noise Ratios for 0 gram per liter hydroxyapatite powder concentration

Level	Discharge Current	Time-On	Time-Off	Gap Voltage
1	23.19	23.38	24.04	24.09
2	24.32	24.24	24.04	24.33
3	25.12	25.01	24.54	24.21
Delta	1.93	1.63	0.5	0.24
Rank	1	2	3	4

Table 12: Response Table for Signal to Noise Ratios for 5 gram per liter hydroxyapatite powder concentration

Level	Discharge Current	Time-On	Time-Off	Gap Voltage
1	25.09	25.68	22.66	23.38
2	23.37	22.73	23.81	23.45
3	21.95	21.99	23.94	23.58
Delta	3.14	3.69	1.28	0.2
Rank	2	1	3	4

Table 11 illustrates that the largest signal to noise ratio is achieved at Level 3 for Discharge Current, Level 3 for Time-On, Level 2 for Time-Off, and Level 1 for Gap Voltage. The rank order of the factors in terms of their impact on Overcut is Discharge Current > Time-On > Time-Off > Gap Voltage, with differences of 1.93, 1.63, 0.5, and 0.24, respectively. On the

other hand, Table 22 shows that the highest signal to noise ratio is achieved at Level 1 for Discharge Current, Level 2 for Time-On, Level 3 for Time-Off, and Level 2 for Gap Voltage. The rank order for the factors in terms of their impact on Overcut is Time-On > Discharge Current > Time-Off > Gap Voltage, with differences of 3.69, 3.14, 1.28, and 0.2, respectively. Comparing the two tables, it is evident that the optimal levels for each factor differ between the two tables, indicating that the concentration of hydroxyapatite powder plays a role in Overcut. Specifically, Discharge Current has the most significant impact in Table 11, while Time-On has the most substantial influence in Table 12. Furthermore, the difference between the highest and lowest signal to noise ratio is more significant in Table 12, suggesting that the variation in the factors has a more considerable impact on Overcut in this case. In conclusion, it can be stated that both the concentration of hydroxyapatite powder and the specific process factors significantly affect Overcut in the macro EDM process. Optimal settings for each factor may differ depending on the powder concentration, and it may be necessary to optimize each factor for each specific powder concentration to achieve the desired Overcut. Figure 10 shows the captures of the Ti-6Al-4V holes after EDM treatment.

The conducted experiments yielded key findings regarding the impact of individual parameters on MRR (material removal rate) and overcut. Specifically, an increase in gap voltage, pulse current, and time on led to a higher MRR due to a corresponding increase in discharge energy and duration. Additionally, a significant rise in TW was observed at low time on values. Other important observations from the experiments include the following:

- The success of the trial is heavily dependent on servo speed, which not only controls the speed but also the backtrack of the tool electrode.
- When the flushing system fails to remove all debris from inside the hole, the feedback system installed in the machine attempts to move the electrode up to avoid a short circuit.
- A low servo speed can cause the electrode to become welded to the tip, resulting in blockage of the dielectric fluid.
- Removing debris at the end of a through hole presents a challenge since no flushing is provided from the tubular electrode.
- The aspect ratio (AR) between hole diameter and depth can complicate debris removal, as failure to remove debris may cause the electrode tip to become welded.

- Any misalignment of the electrode may lead to unfavorable outcomes, including imprecise results, welding, and bending of the tool.
- Higher flushing pressure results in faster machining.

In summary, the experiments shed light on the complex interplay between various parameters and their effects on MRR and TW, as well as on the importance of proper equipment maintenance and operation to ensure optimal results.

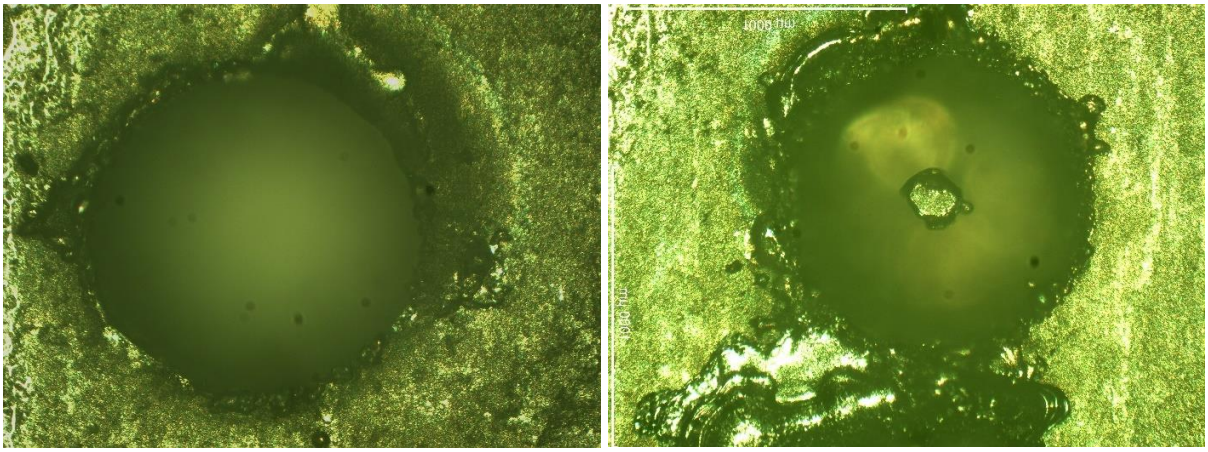

Figure 10: Microscope photos of the through (left) and the blind holes (right) of Ti-6Al-4V alloy by using macro EDM (magnification of 5X)

4.2 Micro EDM

The effects of Capacitance, Voltage, and Powder Concentration on Material Removal Rate (MRR) and overcut were investigated using a Design of Experiment (DOE) approach. The results showed that the levels of the factors had a significant effect on both MRR and Overcut.

Table 13: MRR and Overcut values for different levels of Capacitance, Voltage, and Powder Concentration

Capacitance	Voltage	Powder concentration	MRR (µm^3/s)	Overcut (µm)
3	90	0	33142.50	9.500
3	90	0	30397.36	9.500
3	90	0	30833.39	9.000
3	100	5	69984.63	12.500
3	100	5	67172.75	14.500
3	100	5	68706.38	13.000
3	110	10	72339.89	13.000
3	110	10	65420.42	14.500

3	110	10	65706.10	14.000
4	90	5	9064.27	18.000
4	90	5	7886.11	18.000
4	90	5	7781.09	18.000
4	100	10	9421.85	17.000
4	100	10	13222.05	19.500
4	100	10	14023.01	18.500
4	110	0	14665.39	16.500
4	110	0	14481.90	16.000
4	110	0	16571.25	16.500
5	90	10	43362.24	26.500
5	90	10	43487.56	27.000
5	90	10	48072.51	27.500
5	100	0	61920.56	24.500
5	100	0	62694.57	23.500
5	100	0	64856.45	24.000
5	110	5	58547.46	27.500
5	110	5	63757.19	27.500
5	110	5	69021.54	26.000

Table 13 shows the values of MRR and Overcut at different levels of Capacitance, Voltage, and Powder Concentration. The MRR values ranged from 7,781.097 to 69,984.639 µm^3/s, while the Overcut values ranged from 9.0 to 27.5 µm. The highest MRR value was obtained at a capacitance level of 5, voltage level of 110, and powder concentration level of 5.

4.2.1 MRR

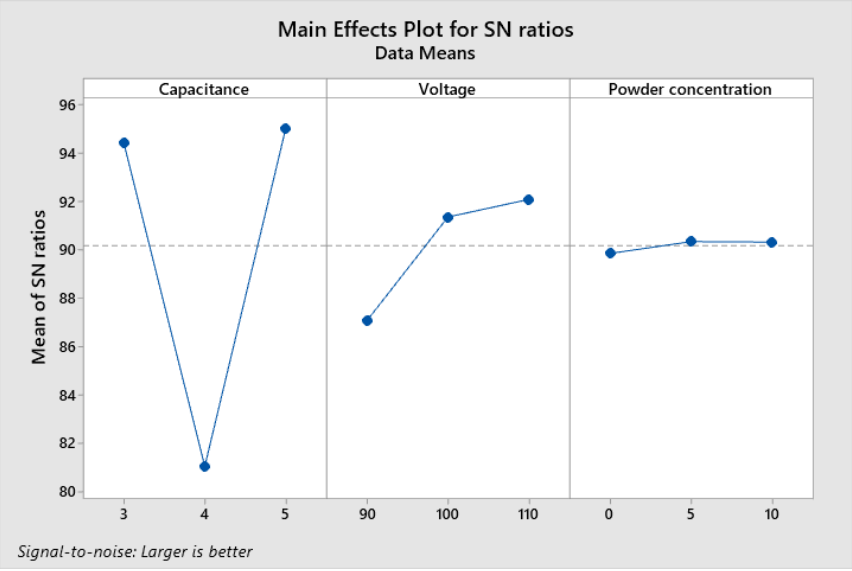

Figure 11: Mean of SN ratios for MRR versus Capacitance, Voltage, and Powder Concentration

Table 14: Response table for Signal to Noise Ratios for Material Removal Rate (MRR) versus Capacitance, Voltage, and Powder Concentration

Level	Capacitance	Voltage	Powder concentration
1	94.42	87.08	89.85
2	81.07	91.35	90.34
3	95.02	92.08	90.32
Delta	13.95	5.01	0.49
Rank	1	2	3

Table 14 displays the signal to noise ratios for the input variables, capacitance, voltage, and powder concentration, at three different levels (1, 2, and 3), with the larger signal to noise ratios indicating better results. The "delta" column shows the difference between the largest and smallest signal to noise ratios for each input variable, and the "rank" column shows the ranking of the input variables based on their signal to noise ratios. The table 14 reveals that the highest signal to noise ratio for MRR was obtained at level 3 of capacitance (95.02), followed by level 2 of voltage (91.35), and level 3 of powder concentration (90.32). This suggests that increasing the capacitance level had the most significant effect on increasing the MRR.

Additionally, the delta values for capacitance, voltage, and powder concentration were 13.95, 5.01, and 0.49, respectively. This indicates that changing the capacitance level had the most significant impact on the MRR, followed by voltage, and then powder concentration. The ranking of the input variables shows that capacitance was the most important input variable for achieving a high MRR in PMEDM of titanium alloys. Therefore, in optimizing the PMEDM process parameters, increasing the capacitance level should be prioritized.

Table 15: Analysis of Variance (ANOVA) table for MRR versus Capacitance, Voltage, and Powder Concentration

Source	DF	Adj SS	Adj MS	F-Value	P-Value
Capacitance	2	12014140327	6007070163	183.88	0
Voltage	2	2463848020	1231924010	37.71	0
Powder concentration	2	473924286	236962143	7.25	0.004
Error	20	653369800	32668490		
Lack-of-Fit	2	524727541	262363770	36.71	0
Pure Error	18	128642259	7146792		

Total	26	15605282432			

Table 15 presents an in-depth analysis of the impact of Capacitance, Voltage, and Powder concentration on Material Removal Rate (MRR). This table helps to identify various sources of variation and their respective contributions to the variation in the response variable (MRR). It is divided into several parts, each depicting a specific aspect of the analysis. The first part of the table identifies the sources of variation, which include Capacitance, Voltage, and Powder concentration. The second part displays the degrees of freedom, which is the difference between the number of observations and the number of parameters being estimated. The third part showcases the adjusted sum of squares (Adj SS), which is a measure of the variation explained by each source of variation, accounting for the variation due to other sources of variation. The fourth part demonstrates the adjusted mean square (Adj MS), calculated by dividing the adjusted sum of squares by the degrees of freedom.

The fifth part of the table provides the F-value, which represents the ratio of the variability between groups to the variability within groups. The F-value is computed by dividing the adjusted mean square for each source of variation by the mean square error (MSE), which measures the variation not explained by any of the sources of variation. The significance of the effect of each source of variation on the response variable is indicated by the F-value, where a higher F-value implies a more significant effect. Lastly, the P-value, which is the probability of observing a result as extreme as the one obtained if the null hypothesis (no effect of the source of variation on the response variable) were true, is presented.

Based on the ANOVA table, it is evident that Capacitance, Voltage, and Powder concentration have a significant impact on MRR. Their low P-values indicate that they are statistically significant in affecting MRR. Capacitance has the highest F-value and P-value among the three sources of variation, indicating that it has the most substantial impact on MRR. Therefore, increasing Capacitance level will lead to a significant increase in MRR. The impact of Voltage on MRR is also significant, although to a lesser extent than Capacitance. Even though Powder concentration has the least significant effect on MRR among the three sources of variation, it is still statistically significant. Hence, all three sources of variation

should be considered while optimizing the PMEDM process parameters for achieving high MRR in titanium alloys.

4.2.2 Overcut

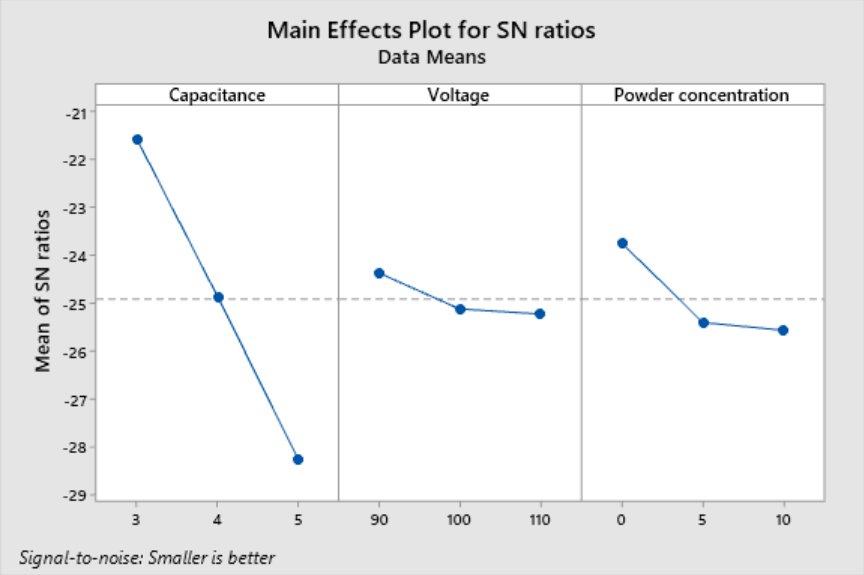

Figure 12: Mean of SN ratios for Overcut versus Capacitance, Voltage, and Powder Concentration

Table 16: Response table for Signal to Noise Ratios for Overcut versus Capacitance, Voltage, and Powder Concentration

Level	Capacitance	Voltage	Powder concentration
1	-21.58	-24.38	-23.76
2	-24.88	-25.13	-25.42
3	-28.29	-25.24	-25.58
Delta	6.71	0.86	1.82
Rank	1	3	2

Table 16 shows the signal to noise ratios for Overcut with respect to the input variables Capacitance, Voltage, and Powder Concentration. In this table, smaller values are better, as the objective is to minimize the overcut. It shows the S/N ratios for each level of the input variables and the rank based on the delta value.

From the Table 16, it can be observed that the lowest S/N ratios are obtained at level 1 for all three input variables, indicating that a lower value of capacitance, voltage, and powder

concentration is beneficial for reducing the overcut. The delta values show that capacitance has the most significant effect on the overcut, followed by powder concentration and voltage. The rank order indicates that level 1 of capacitance is the most effective in minimizing the overcut, followed by level 3 of powder concentration and level 2 of voltage. These results suggest that reducing the capacitance and powder concentration and increasing the voltage can help to minimize the overcut during PMEDM.

Table 17: Analysis of Variance (ANOVA) table for Overcut versus Capacitance, Voltage, and Powder Concentration

Source	DF	Adj SS	Adj MS	F-Value	P-Value
Capacitance	2	875.13	437.56	770.91	0
Voltage	2	4.019	2.00	3.54	0.048
Powder concentration	2	55.352	27.67	48.76	0
Error	20	11.352	0.56		
Lack-of-Fit	2	2.019	1.0	1.95	0.172
Pure Error	18	9.333	0.52		
Total	26	945.852			

The ANOVA analysis reveals that all three independent variables, namely Capacitance, Voltage, and Powder concentration, significantly affect the overcut. The P-values for all three variables are less than 0.05, which means that the null hypothesis that there is no effect of the variable on the overcut can be rejected with 95% confidence. Capacitance has the highest F-value and the lowest P-value among the three variables, indicating that it has the largest effect on the overcut.

Table 17 also includes an analysis of the Error term, which represents the unexplained variability in the data. The Lack-of-Fit term assesses whether the model fits the data appropriately, while the Pure Error term represents the variability that cannot be attributed to any source of variation in the model. The Lack-of-Fit term has a relatively high P-value, indicating that the model fits the data well.

In conclusion, the ANOVA results suggest that capacitance, voltage, and powder concentration significantly influence the overcut in the machining process.

4.3 Optical microscope and SEM

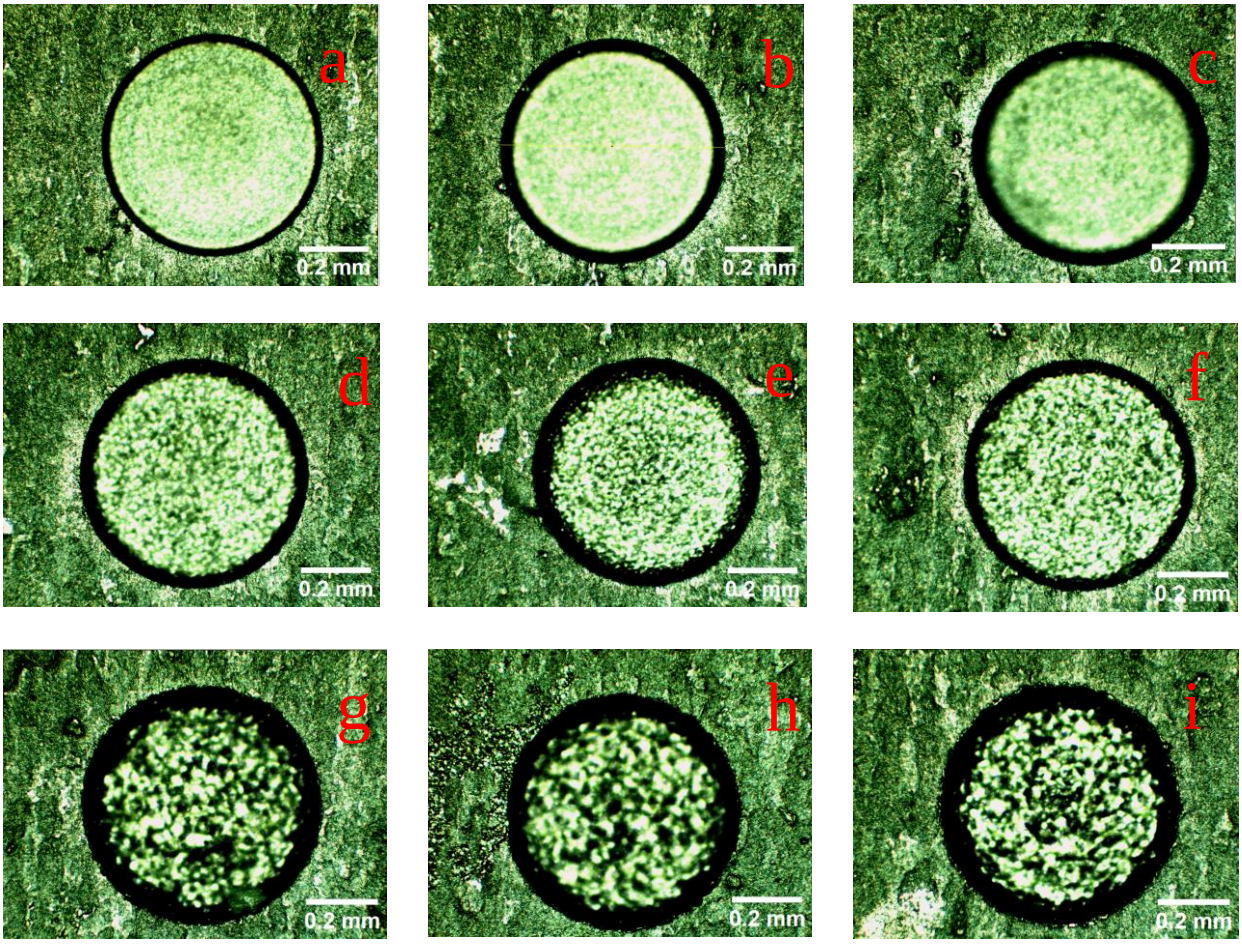

Figure 13: Optical microscope captures of micro-EDM treated Ti-6Al-4V holes using tungsten carbide electrode tool for different discharge energies; (a) 100pF, 90V, (b) 100pF, 100V, (c) 100 pF, 110V, (d) 1nF, 90V, (e) 1nF, 100V, (f) 1nF, 110V, (g) 10nF, 90V, (h) 10nF, 100V, (i) 10nF, 110V at constant electrode rotational speed of 1000 rpm.

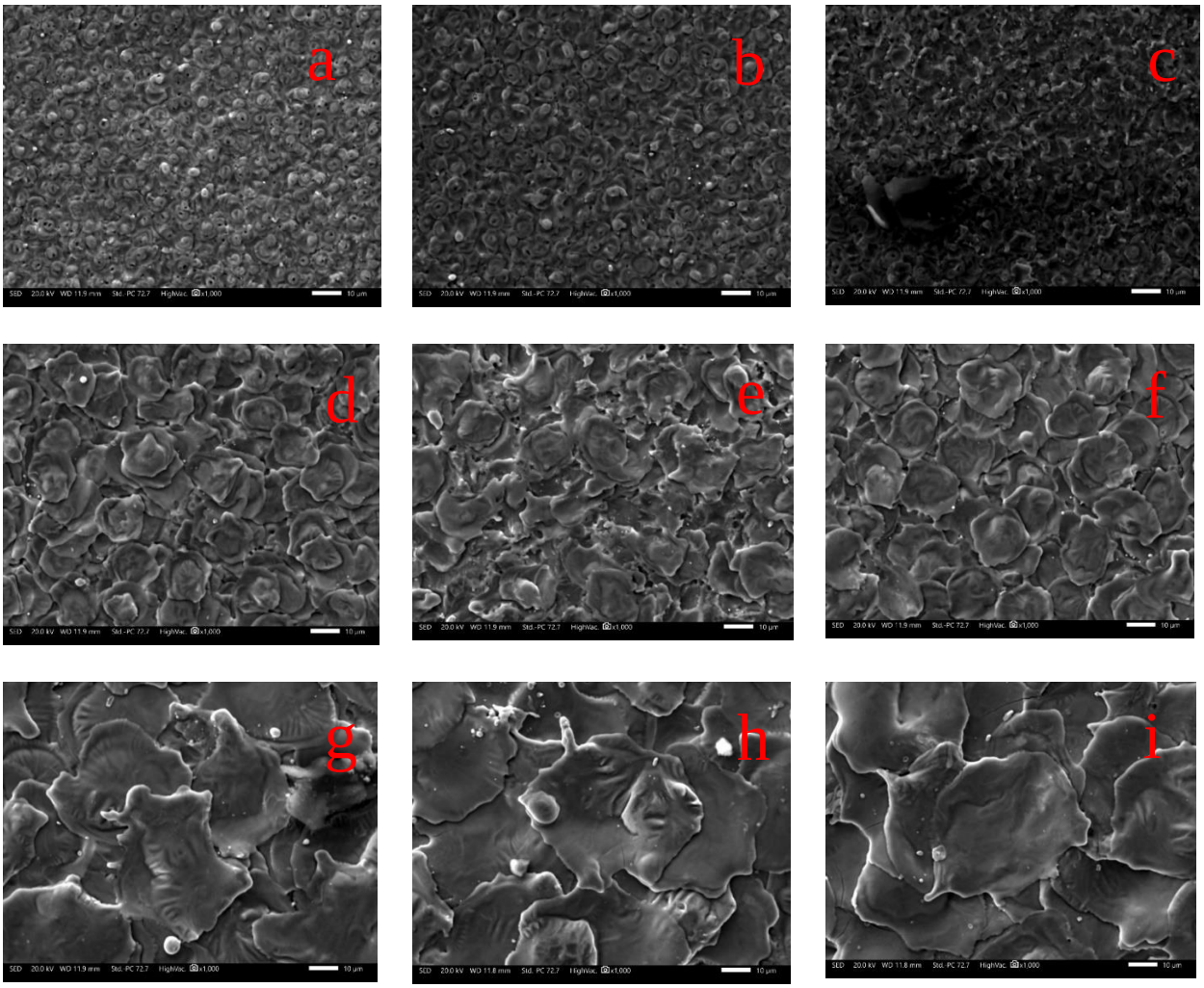

Figure 14: SEM captures for different discharge energies for micro-EDM of Ti-6Al-4V using tungsten carbide electrode tool; (a) 100pF, 90V, (b) 100pF, 100V, (c) 100 pF, 110V, (d) 1nF, 90V, (e) 1nF, 100V, (f) 1nF, 110V, (g) 10nF, 90V, (h) 10nF, 100V, (i) 10nF, 110V at constant electrode rotational speed of 1000 rpm.

Table 18: Elemental analysis of Ti-6Al-4V plate before and after micro-EDM treatment

Element	Line	Mass%	Atom%
Al	K	2.87±0.01	6.00±0.02
P	K	0.18±0.00	0.33±0.01
Ca	K	0.02±0.00	0.03±0.00
Ti	K	70.46±0.04	82.90±0.05
V	K	3.15±0.01	3.49±0.01
Co	K	0.17±0.01	0.16±0.01
W	M	23.14±0.04	7.09±0.01
Total		100	100
		Fitting ratio 0.045	

Element	Line	Mass%	Atom%
Al	K	5.7±0.01	9.65±0.02
Ti	K	89.45±0.04	85.19±0.04
V	K	3.82±0.01	3.42±0.01
Na	K	0.64±0.01	1.26±0.01
Cl	K	0.29±0.00	0.38±0.00
K	K	0.10±0.00	0.11±0.00
Total		100	100
		Fitting ratio 0.0073	

In the present study, micro-EDM treatment was applied to Ti-6Al-4V samples, and SEM captures, and EDS analysis were performed to investigate the elemental composition of the machined holes. Table 18 represents the EDS analysis before and after micro-EDM treatment. The results indicate that, in addition to the primary constituents of Ti, Al, and V, there was evidence of material transfer from the tungsten carbide electrode and hydroxyapatite powder in the dielectric. Specifically, tungsten was identified as originating from the electrode, while the presence of calcium and phosphorus was attributed to the hydroxyapatite powder. It should be noted that the Ti-6Al-4V alloy used in this study had a chemical composition of 90 wt.% Ti, 6 wt.% Al, 4 wt.% V, 0.2 wt.% O, and 0.05 wt.% N, according to Table 5. The chemical composition of hydroxyapatite is Ca5(PO4)3(OH). These findings suggest that the material transfer observed during micro-EDM treatment may have resulted from a combination of electrode wear and contamination from the dielectric fluid. Further investigations are needed to understand the extent of this material transfer and its potential implications for the performance and properties of the treated Ti-6Al-4V samples.

4.4 Crater Size

The aim of this study was to investigate the effect of input parameters, namely capacitance, voltage, and powder concentration, on the crater size during micro-EDM machining on Ti-6Al-4V in hydrocarbon dielectric. The results were analyzed by measuring the crater area for each experimental set using ImageJ software. The data were captured in x1000 magnification

in order to clearly observe the difference in crater size with the change of input parameters. Table 19 presents the crater area [μm^2] values for different levels of capacitance, voltage, and powder concentration. The data were estimated using Minitab software. It is evident that the crater area is affected by the input parameters. For instance, according to figure 12, with an increase in capacitance from 3 to 4, there is a steady increase in the crater size, whereas from 4 to 5, there is a significant increase in crater size. Similarly, there is a constant increase in crater size with an increase in voltage. The effect of powder concentration on crater size is moderate, with a slight increase in crater size from 0 to 5, and a moderate decrease in crater size from 5 to 10.

Table 19: Crater area values for different levels of Capacitance, Voltage, and Powder Concentration

Capacitance	**Voltage [V]**	**Powder concentration [g/l]**	**Crater area [μm^2]**
3	90	0	34.116
3	100	5	42.5024
3	110	10	41.8264
4	90	5	217.3106
4	100	10	263.9776
4	110	0	317.8454
5	90	10	1354.609333
5	100	0	2111.6435
5	110	5	2877.3125

Figure 15: Mean of SN ratios for crater area values versus Capacitance, Voltage, and Powder Concentration

Table 20: Response table for Signal to Noise Ratios for Overcut versus Capacitance, Voltage, and Powder Concentration

Level	Capacitance	Voltage	Powder concentration
1	39.48	535.35	821.2
2	266.38	806.04	1045.71
3	2114.52	1078.99	553.47
Delta	2075.04	543.65	492.24
Rank	1	2	3

The results were further analyzed using the signal-to-noise (SN) ratio approach. Table 20 presents the response table for SN ratios for overcut versus capacitance, voltage, and powder concentration. The delta values indicate the degree of influence of each parameter on the response, with the highest value corresponding to the most influential parameter. The results indicate that capacitance is the most influential parameter, followed by voltage and powder concentration.

The results of this study indicate that the input parameters, namely capacitance, voltage, and powder concentration, have a significant impact on the crater size during micro-EDM machining on Ti-6Al-4V in hydrocarbon dielectric. The findings suggest that increasing the

capacitance and voltage can lead to an increase in crater size, while the effect of powder concentration is moderate. These findings can help in optimizing the micro EDM machining process for Ti-6Al-4V in hydrocarbon dielectric.

4.5 Hardness test results

The present study includes an analysis of untreated bulk Ti-6Al-4V alloy, which has a hardness range of 444.93 to 528.42, with an average hardness value of 502.374, serving as a baseline for comparison to the hardness values obtained from the holes on Ti-6Al-4V titanium samples machined by micro EDM with and without the addition of powder.

Table 21: Hardness values for all experiments

Capacitance	Voltage	Powder concentration	Hardness 1 [HV/0.2]	Hardness 2 [HV/0.2]	Hardness 3 [HV/0.2]	Average hardness [HV/0.2]
3	90	0	340.3	347.94	345.34	344.53
3	90	0	340.99	332.9	346.77	340.22
3	90	0	448.96	399.21	398.25	415.47
3	100	5	356.93	349.12	356.82	354.29
3	100	5	355.73	350.23	353.4	353.12
3	100	5	350.4	354.49	356.53	353.81
3	110	10	383.73	343.32	374.74	367.26
3	110	10	423.16	454.32	499.09	458.86
3	110	10	363.92	360.31	359.42	361.22
4	90	5	343.6	368.93	371.15	361.23
4	90	5	373.85	369.78	394.67	379.43
4	90	5	362.24	362.39	375.03	366.55
4	100	10	394.47	404.8	376.05	391.77
4	100	10	397.22	378.3	392.5	389.34
4	100	10	403.73	400.33	415.04	406.36
4	110	0	377.84	354.83	353.46	362.04
4	110	0	386.76	386.68	377.94	383.79
4	110	0	367.33	507.28	444.49	439.70
5	90	10	396.16	422.4	409.7	409.42
5	90	10	408.99	403.32	441.61	417.97
5	90	10	371.12	441.75	408.58	407.15
5	100	0	388.39	394.33	452.68	411.80
5	100	0	396.08	482.6	367.95	415.54
5	100	0	415.29	360.59	369.71	381.86
5	110	5	379.91	416.15	362.87	386.31

5	110	5	389.65	392.88	381.33	387.95
5	110	5	457.91	417.64	460.97	445.51

Upon examining the data in Table 21, it can be observed that hardness values obtained from the experiments varied based on the levels of capacitance, voltage, and powder concentration. The highest average hardness value of 445.5066667 was obtained at level 5 with a capacitance of 5, a voltage of 110, and a powder concentration of 5, followed by an average hardness value of 439.7 obtained at level 4 with a capacitance of 4, a voltage of 110, and a powder concentration of 0.

Interestingly, the addition of powder to the EDM process did not always result in an increase in hardness. For instance, at level 3, with a capacitance of 3, a voltage of 90, and a powder concentration of 0, the average hardness value obtained was 344.5266667, which is lower than the hardness value obtained without powder at level 5.

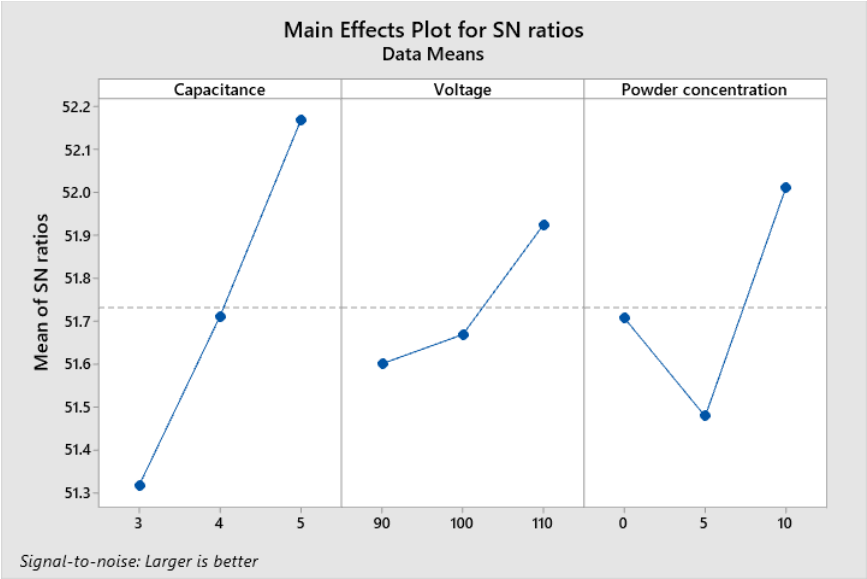

Figure 16: Mean of SN ratios for surface hardness values versus Capacitance, Voltage, and Powder Concentration

Table 22: Response Table for Signal to Noise Ratios for surface hardness values versus Capacitance, Voltage, and Powder Concentration

Level	Capacitance	Voltage	Powder concentration
1	51.32	51.60	51.71
2	51.71	51.67	51.48

3	52.17	51.93	52.01
Delta	0.85	0.32	0.53
Rank	1	3	2

Further analysis of the data can be conducted by referring to the table 22 for signal-to-noise ratios. It is evident that the highest value for all three factors was obtained at level 3, with a delta of 0.85. This finding suggests that capacitance level 3 produced the most consistent and reliable results compared to the other levels.

To conclude, the results from the Falcon 300 hardness tester for Ti-6Al-4V titanium samples machined by micro EDM with and without the addition of powder demonstrate considerable variations depending on the experimental conditions employed. The highest average hardness values were observed at level 5 and 4, and the addition of powder did not always lead to an increase in hardness. The response table for signal-to-noise ratios indicates that level 3 generated the most consistent and reliable outcomes. These outcomes offer valuable insights for future studies aimed at optimizing the micro EDM process for Ti-6Al-4V titanium samples.

It is important to note that the present study employed tungsten carbide electrodes in micro EDM, which may have led to the deposition of some of the carbide on the treated surface. This could potentially increase the hardness value in some of the experimental trials and adversely affect the consistency of results.

4.6 Surface roughness

Surface hardness is a critical characteristic that determines the mechanical strength of materials. In this study, the surface hardness of Ti-6Al-4V samples treated with micro wire EDM was investigated by varying the input parameters. The input parameters included discharge energy and hydroxyapatite powder concentration in the hydrocarbon dielectric.

Table 23: Surface roughness measurements for micro wire EDM treated Ti-6Al-4V workpieces.

Energy	**powder**	**Roughness 1 [µm]**	**Roughness 2 [µm]**	**Roughness 3 [µm]**	**Average roughness [µm]**
Low	0	0.295	0.279	0.243	0.27
medium	0	0.667	0.715	0.719	0.70
High	0	1.763	1.715	1.567	1.68

low	5	0.274	0.249	0.343	0.29
Medium	5	0.642	0.675	0.644	0.65
High	5	1.71	1.861	1.745	1.77
low	10	0.247	0.234	0.413	0.29
medium	10	0.754	0.869	0.627	0.75
High	10	1.832	1.737	1.56	1.71

To measure the surface hardness, the surface roughness of the treated samples was analyzed. Three experiments were conducted for each combination of input parameters, and the average surface roughness values were calculated. Table 23Table 23: Surface roughness measurements for micro wire EDM treated Ti-6Al-4V workpieces. shows the surface roughness measurements for the micro wire EDM treated Ti-6Al-4V workpieces.

The results indicate that the surface roughness values varied significantly depending on the input parameters. The average surface roughness values for low, medium, and high discharge energy with 0 g/L hydroxyapatite powder concentration were 0.272333, 0.700333, and 1.681667, respectively. Similarly, for 5 g/L and 10 g/L hydroxyapatite powder concentrations, the average surface roughness values increased with the increase in discharge energy.

Furthermore, the hydroxyapatite powder concentration also affected the surface roughness values. For all three discharge energies, the average surface roughness values increased with the increase in hydroxyapatite powder concentration. For instance, at high discharge energy, the average surface roughness values were 1.709667, 1.772, and 1.832 for 0 g/L, 5 g/L, and 10 g/L hydroxyapatite powder concentrations, respectively.

In conclusion, the surface hardness of Ti-6Al-4V samples treated with micro wire EDM can be controlled by varying the input parameters. The results of this study suggest that higher discharge energy and hydroxyapatite powder concentration lead to higher surface roughness values, which may indicate higher surface hardness. However, further studies are required to determine the precise relationship between surface roughness and surface hardness.

4.7 Contact angle

The contact angle of a liquid on a solid surface is a fundamental property that is influenced by various factors, including the surface roughness and the input parameters used during the treatment of the solid surface. In this study, the contact angle of Ti-6Al-4V samples treated with micro wire EDM was measured using the sessile drop method. The input parameters

that were varied included discharge energy and hydroxyapatite powder concentration in the hydrocarbon dielectric. Three experiments were conducted for each combination of input parameters, and the average contact angle was calculated.

Table 24: Surface contact angle measurements for micro wire EDM treated Ti-6Al-4V workpieces.

Energy	Powder (0, 5, 10 g/l)	contact angle 1 [˚]	contact angle 2 [˚]	contact angle 3 [˚]	Average contact angle [˚]
Low	0	52.8	49.7	61.5	54.67
medium	0	52.1	51.4	51	51.50
High	0	55.8	55.8	51.1	54.23
low	5	54.4	40.3	47.8	47.50
Medium	5	47	51	66.1	54.70
High	5	59.6	58.5	56.2	58.10
low	10	43.6	47.6	45.4	45.53
medium	10	64	60.5	54.2	59.57
High	10	44.7	58.3	62.8	55.27

The results, according to table 24, showed that the average contact angle values varied between 45.53° and 59.57° depending on the input parameters used. Specifically, the highest average contact angle value of 59.57° was obtained for the medium energy input and a hydroxyapatite powder concentration of 10 g/l. Conversely, the lowest average contact angle value of 45.53° was obtained for the low energy input and a hydroxyapatite powder concentration of 10 g/l.

Interestingly, the surface roughness values also showed a notable effect on the contact angle values. The roughness values ranged from 0.247 to 1.832, and a higher roughness was generally associated with a higher contact angle value. For instance, the highest surface roughness value of 1.832 was obtained for the high energy input and a hydroxyapatite powder concentration of 10 g/l, which corresponded to an average contact angle of 55.27°. On the other hand, the lowest surface roughness value of 0.234 was obtained for the medium energy input and a hydroxyapatite powder concentration of 10 g/l, which corresponded to an average contact angle of 59.57°.

In summary, surface roughness can significantly affect the contact angle of a surface. In general, the presence of surface roughness can increase the contact angle of a liquid droplet on a

surface. This effect is due to the fact that surface roughness increases the surface area and can create more surface defects and microstructures that can trap air or other materials between the solid and liquid phases. This leads to a reduction in the solid-liquid contact area and an increase in the apparent contact angle.

4.8 Biological attachments

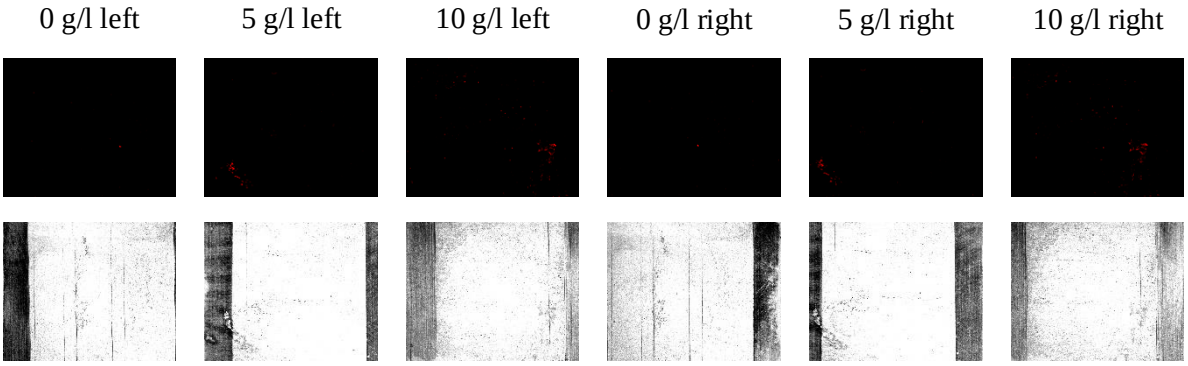

Figure 17: Crystal Violet stained and Brightfield pictures of Staphylococcus aureus bacterial attachment on machined Ti-6Al-4V alloy with low energy (100pF, 90 V) for left and right cuts.

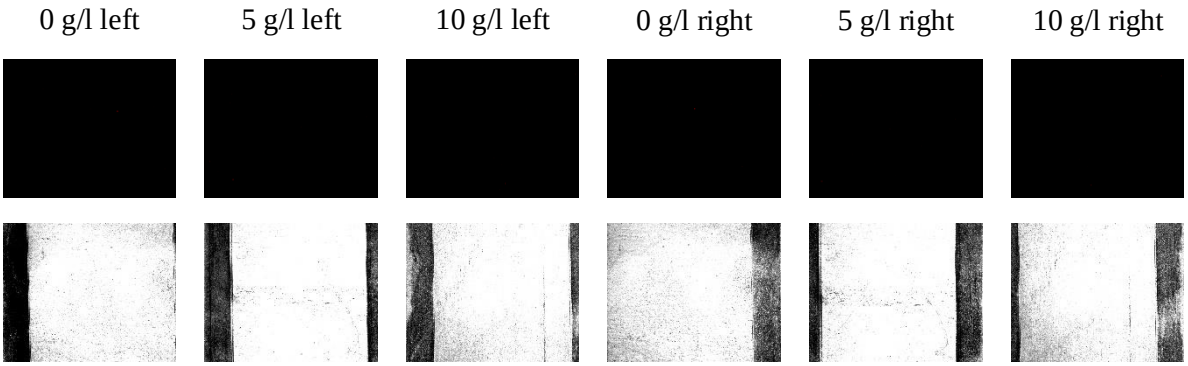

Figure 18: Crystal Violet stained and Brightfield pictures of Staphylococcus aureus bacterial attachment on machined Ti-6Al-4V alloy with medium energy (1nF, 100 V) for left and right cuts.

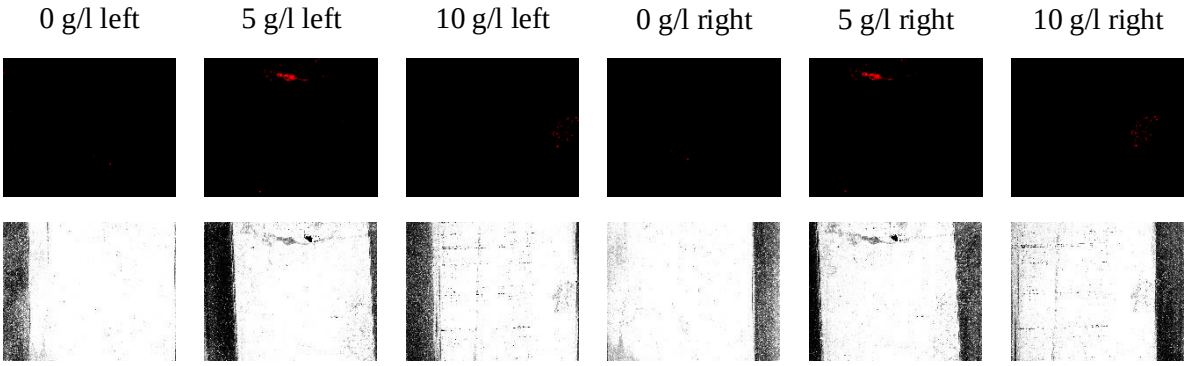

Figure 19: Crystal Violet stained and Brightfield pictures of Staphylococcus aureus bacterial attachment on machined Ti-6Al-4V alloy with high energy (10 nF, 110 V) for left and right cuts.

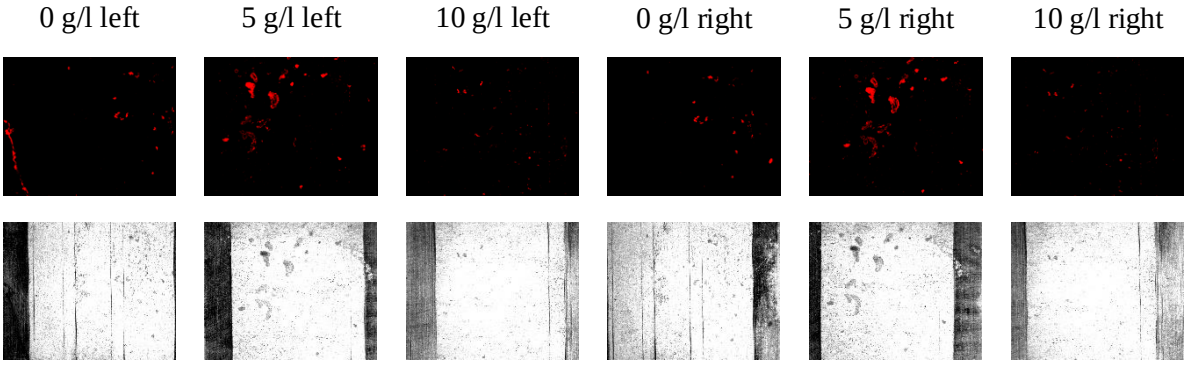

Figure 20: Crystal Violet stained and Brightfield pictures of Escherichia Coli bacterial attachment on machined Ti-6Al-4V alloy with low energy (100pF, 90 V) for left and right cuts.

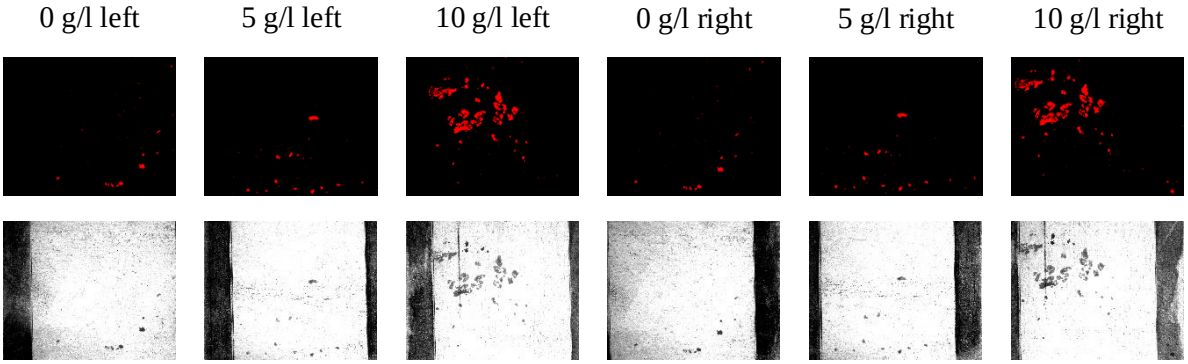

Figure 21: Crystal Violet stained and Brightfield pictures of Escherichia Coli bacterial attachment on machined Ti-6Al-4V alloy with medium energy (1nF, 100 V) for left and right cuts.

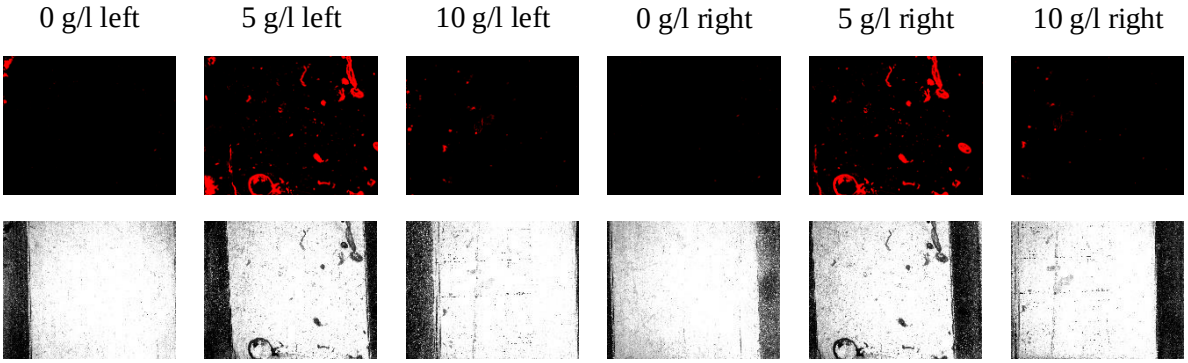

Figure 22: Crystal Violet stained and Brightfield pictures of Escherichia Coli bacterial attachment on machined Ti-6Al-4V alloy with high energy (10nF, 110 V) for left and right cuts.

The present study aimed to investigate the effect of powder mixed Wire EDM on the biocompatibility of Ti-6Al-4V alloy against bacterial strains, namely Staphylococcus aureus and Escherichia coli. The bacterial biofilm formation was assessed using crystal violet staining method after incubation of bacterial strains on machined and unmachined surfaces of the Ti-6Al-4V alloy.

According to figures 17-22, it can be seen that the discharge energy settings had a significant effect on the bacterial adhesion properties. For low energy results, tiny colonies of bacteria were observed on the unmachined surface for all the bacterial strains, while no bacterial adhesion was observed on the machined surface of Ti-6Al-4V alloy against Staphylococcus aureus. However, for medium and high energy settings, almost no bacterial adhesion was observed on the machined surface of Ti-6Al-4V alloy for all bacterial strains.

Furthermore, the hydroxyapatite powder concentration also played a crucial role in bacterial adhesion. For instance, for Escherichia Coli, no bacterial adhesion was observed on the machined surface for 10g/l hydroxyapatite powder concentration for all energy settings. However, for 0g/l and 5g/l hydroxyapatite powder concentrations, bacterial adhesion was observed on the machined surface for low and high energy settings.

Interestingly, the results also showed that the unmachined surface of Ti-6Al-4V alloy had a higher tendency for bacterial adhesion compared to the machined surface. For instance, for Escherichia coli, bacterial adhesion was observed on the unmachined surface for all energy settings and hydroxyapatite powder concentrations, while for the machined surface, bacterial adhesion was observed only for 0g/l and 5g/l hydroxyapatite powder concentrations for low energy settings.

In conclusion, the present study suggests that powder mixed Wire EDM machining technique can be an effective method to improve the biocompatibility of Ti-6Al-4V alloy against bacterial strains, particularly for high energy settings and higher hydroxyapatite powder concentrations. These findings have potential implications for the development of biomedical implants with enhanced antibacterial properties. However, further studies are needed to validate these results and investigate the long-term effects of powder mixed Wire EDM machining technique on the biocompatibility of Ti-6Al-4V alloy.

Chapter 5 – Conclusion

In conclusion, the research aims to develop a thorough understanding of Powder Mixed EDM machining performance on Ti-6Al-4V and improve its surface biocompatibility. To accomplish this, a systematic investigation was conducted on multi-scale EDM machines with four specific objectives.

The results of the macro-EDM experiments suggest that careful selection and optimization of input parameters and powder additive concentration in the dielectric can significantly improve the performance of macro EDM on Ti-6Al-4V titanium alloy. Similarly, for micro EDM machining, optimizing the input variables of capacitance, voltage, and powder concentration can improve the efficiency and quality of micro EDM machining processes. The bacterial attachment experiments also revealed that the input parameters had a significant effect on bacterial attachment, and a combination of medium and high energy input, high hydroxyapatite powder concentration, and low surface roughness can lead to the lowest bacterial attachment on the micro wire EDM machined parts. Furthermore, medium, and high energy settings are more effective in preventing bacterial adhesion on the machined surface of Ti-6Al-4V alloy for all bacterial strains.

It is noteworthy that the machined surface had lower bacterial adhesion compared to the unmachined surface of the alloy, indicating that micro wire EDM machining can be an effective method in reducing bacterial adhesion on metallic surfaces. The SEM and EDS results also indicate that a proper combination of base material, electrode tool, dielectric, and powder additive in micro EDM machining can enhance biocompatibility. Therefore, the findings of this research have significant implications for biomedical applications of Ti-6Al-4V titanium alloy.

In conclusion, the findings of this research have shown that optimizing the input parameters and dielectric concentration can significantly improve the performance of Powder Mixed EDM machining on Ti-6Al-4V titanium alloy. The results also suggest that Powder Mixed EDM machining can be an effective method for improving surface biocompatibility, and micro wire EDM machining can be an effective method in reducing bacterial adhesion on metallic surfaces. These findings are relevant and significant for biomedical applications of Ti-6Al-4V titanium alloy, where biocompatibility and bacterial attachment are crucial factors.

Further studies can build on these findings and investigate the effectiveness of Powder Mixed EDM machining on other metallic materials and its potential applications in various biomedical fields.

References

[1] V. D. Bui, J. W. Mwangi, and A. J. J. o. M. P. Schubert, "Powder mixed electrical discharge machining for antibacterial coating on titanium implant surfaces," vol. 44, pp. 261-270, 2019.

[2] M. Navarro, A. Michiardi, O. Castano, and J. J. J. o. t. r. s. i. Planell, "Biomaterials in orthopaedics," vol. 5, no. 27, pp. 1137-1158, 2008.

[3] C. Lhotka, T. Szekeres, I. Steffan, K. Zhuber, and K. J. J. o. O. R. Zweymüller, "Four-year study of cobalt and chromium blood levels in patients managed with two different metal-on-metal total hip replacements," vol. 21, no. 2, pp. 189-195, 2003.

[4] Z. Wang, Y. Fang, P. Wu, W. Zhao, and K. J. J. o. M. P. T. Cheng, "Surface modification process by electrical discharge machining with a Ti powder green compact electrode," vol. 129, no. 1-3, pp. 139-142, 2002.

[5] N. M. Abbas, D. G. Solomon, M. F. J. I. J. o. m. t. Bahari, and Manufacture, "A review on current research trends in electrical discharge machining (EDM)," vol. 47, no. 7-8, pp. 1214-1228, 2007.

[6] S. Kumar, R. Singh, T. P. Singh, and B. J. J. o. M. P. T. Sethi, "Surface modification by electrical discharge machining: A review," vol. 209, no. 8, pp. 3675-3687, 2009.

[7] M. Tanjilul, A. Ahmed, A. S. Kumar, and M. Rahman, "A study on EDM debris particle size and flushing mechanism for efficient debris removal in EDM-drilling of Inconel 718," *Journal of Materials Processing Technology,* vol. 255, pp. 263-274, 2018.

[8] J. E. Abu Qudeiri, A.-H. I. Mourad, A. Ziout, M. H. Abidi, and A. Elkaseer, "Electric discharge machining of titanium and its alloys," *The international journal of advanced manufacturing technology,* vol. 96, no. 1, pp. 1319-1339, 2018.

[9] A. Kumar, A. Mandal, A. R. Dixit, and A. K. Das, "Performance evaluation of Al2O3 nano powder mixed dielectric for electric discharge machining of Inconel 825," *Materials and Manufacturing Processes,* vol. 33, no. 9, pp. 986-995, 2018.

[10] T. Muthuramalingam and B. Mohan, "A review on influence of electrical process parameters in EDM process," *Archives of civil and mechanical engineering,* vol. 15, no. 1, pp. 87-94, 2015.

[11] S. Chakraborty, V. Dey, and S. Ghosh, "A review on the use of dielectric fluids and their effects in electrical discharge machining characteristics," *Precision Engineering,* vol. 40, pp. 1-6, 2015.

[12] H. Lim, Y. Wong, M. Rahman, and M. E. J. J. o. M. P. T. Lee, "A study on the machining of high-aspect ratio micro-structures using micro-EDM," vol. 140, no. 1-3, pp. 318-325, 2003.

[13] L. Raju and S. S. J. P. T. Hiremath, "A state-of-the-art review on micro electro-discharge machining," vol. 25, pp. 1281-1288, 2016.

[14] S. Mohanty, V. Kumar, A. K. Das, and A. R. J. J. o. M. P. Dixit, "Surface modification of Ti-alloy by micro-electrical discharge process using tungsten disulphide powder suspension," vol. 37, pp. 28-41, 2019.

[15] M. Kunieda, B. Lauwers, K. P. Rajurkar, and B. M. J. C. a. Schumacher, "Advancing EDM through fundamental insight into the process," vol. 54, no. 2, pp. 64-87, 2005.

[16] D. Buser, R. Schenk, S. Steinemann, J. Fiorellini, C. Fox, and H. J. J. o. b. m. r. Stich, "Influence of surface characteristics on bone integration of titanium implants. A histomorphometric study in miniature pigs," vol. 25, no. 7, pp. 889-902, 1991.

[17] K. Kieswetter, Z. Schwartz, D. Dean, B. J. C. R. i. O. B. Boyan, and Medicine, "The role of implant surface characteristics in the healing of bone," vol. 7, no. 4, pp. 329-345, 1996.

[18] M. P. Jahan, P. Kakavand, and F. J. P. M. Alavi, "A comparative study on micro-electro-discharge-machined surface characteristics of Ni-Ti and Ti-6Al-4V with respect to biocompatibility," vol. 10, pp. 232-242, 2017.

[19] M. P. Jahan, M. Rahman, and Y. S. J. T. I. J. o. A. M. T. Wong, "Study on the nano-powder-mixed sinking and milling micro-EDM of WC-Co," vol. 53, no. 1, pp. 167-180, 2011.

[20] P. Kiran, S. Mohanty, A. K. J. M. Das, and M. Processes, "Surface modification through sustainable micro-EDM process using powder mixed bio-dielectrics," vol. 37, no. 6, pp. 640-651, 2022.
[21] K. Wang, Q. Zhang, G. Zhu, and J. J. T. I. J. o. A. M. T. Zhang, "Effects of tool electrode size on surface characteristics in micro-EDM," vol. 96, no. 9, pp. 3909-3916, 2018.
[22] A. Y. Joshi and A. Y. J. H. Joshi, "A systematic review on powder mixed electrical discharge machining," vol. 5, no. 12, p. e02963, 2019.
[23] M. Al-Amin *et al.*, "Powder mixed-EDM for potential biomedical applications: a critical review," vol. 35, no. 16, pp. 1789-1811, 2020.
[24] H.-M. Chow, L.-D. Yang, C.-T. Lin, and Y.-F. J. J. o. m. p. t. Chen, "The use of SiC powder in water as dielectric for micro-slit EDM machining," vol. 195, no. 1-3, pp. 160-170, 2008.
[25] F. J. J. o. D. U. o. T. Zhao, "Research on effecting mechanism of particles in powder-mixed EDM," vol. 45, no. 5, pp. 668-671, 2005.
[26] C. Prakash, H. K. Kansal, B. Pabla, S. J. J. o. C. Puri, and I. S. i. Engineering, "Powder mixed electric discharge machining: an innovative surface modification technique to enhance fatigue performance and bioactivity of β-Ti implant for orthopedics application," vol. 16, no. 4, 2016.
[27] S. Assarzadeh and M. J. T. I. J. o. A. M. T. Ghoreishi, "A dual response surface-desirability approach to process modeling and optimization of Al 2 O 3 powder-mixed electrical discharge machining (PMEDM) parameters," vol. 64, pp. 1459-1477, 2013.
[28] M. Hourmand, A. A. Sarhan, S. Farahany, and M. Sayuti, "Microstructure characterization and maximization of the material removal rate in nano-powder mixed EDM of Al-Mg2Si metal matrix composite—ANFIS and RSM approaches," *The International Journal of Advanced Manufacturing Technology,* vol. 101, no. 9, pp. 2723-2737, 2019.
[29] S. Gudur and V. Potdar, "Effect of silicon carbide powder mixed EDM on machining characteristics of SS 316L materialexperimentation," *International Journal of Innovation Research in Science, Engineering and Technology,* vol. 4, 2015.
[30] C. Prakash, H. Kansal, B. Pabla, and S. Puri, "Experimental investigations in powder mixed electric discharge machining of Ti–35Nb–7Ta–5Zrβ-titanium alloy," *Materials and Manufacturing Processes,* vol. 32, no. 3, pp. 274-285, 2017.
[31] N. D. Gosai and A. Y. Joshi, "Experimental investigation and optimization of process parameters used in the silicon powder mixed electro discharge machining of Ti-6Al-4V alloy using response surface methodology," *Journal for Manufacturing Science and Production,* vol. 16, no. 1, pp. 21-32, 2016.
[32] T.-L. Banh, H.-P. Nguyen, C. Ngo, and D.-T. Nguyen, "Characteristics optimization of powder mixed electric discharge machining using titanium powder for die steel materials," *Proceedings of the Institution of Mechanical Engineers, Part E: Journal of Process Mechanical Engineering,* vol. 232, no. 3, pp. 281-298, 2018.
[33] M. Kolli and A. Kumar, "Assessing the influence of surfactant and B4C powder mixed in dielectric fluid on EDM of titanium alloy," *Silicon,* vol. 11, no. 4, pp. 1731-1743, 2019.
[34] B. Gugulothu, G. K. M. Rao, and D. H. Rao, "Influence of drinking water and graphite powder concentration on electrical discharge machining of Ti-6Al-4V alloy," *Materials Today: Proceedings,* vol. 27, pp. 294-300, 2020.
[35] S. Omarov, N. Nauryz, D. Talamona, and A. J. M. Perveen, "Surface Modification Techniques for Metallic Biomedical Alloys: A Concise Review," vol. 13, no. 1, p. 82, 2022.
[36] A. A. Khan, M. Y. Ali, M. M. J. I. J. o. M. Haque, and M. Engineering, "A study of electrode shape configuration on the performance of die sinking EDM," vol. 4, no. 1, pp. 19-23, 2009.

[37] Y. Lamichhane, G. Singh, A. S. Bhui, P. Mukhiya, P. Kumar, and B. J. M. T. P. Thapa, "Surface modification of 316L SS with HAp nano-particles using PMEDM for enhanced biocompatibility," vol. 15, pp. 336-343, 2019.

[38] G. Sharma, K. Kumar, P. Satsangi, and N. J. I. Sharma, "Surface modification of biodegradable Mg-4Zn alloy using PMEDM: an experimental investigation, optimization and corrosion analysis," 2021.

[39] L. Murr *et al.*, "Microstructure and mechanical behavior of Ti–6Al–4V produced by rapid-layer manufacturing, for biomedical applications," vol. 2, no. 1, pp. 20-32, 2009.

[40] P. L. Ferrandini, F. F. Cardoso, S. A. Souza, C. R. Afonso, R. J. J. o. A. Caram, and Compounds, "Aging response of the Ti–35Nb–7Zr–5Ta and Ti–35Nb–7Ta alloys," vol. 433, no. 1-2, pp. 207-210, 2007.

[41] S. Joschek, B. Nies, R. Krotz, and A. J. B. Göpferich, "Chemical and physicochemical characterization of porous hydroxyapatite ceramics made of natural bone," vol. 21, no. 16, pp. 1645-1658, 2000.

Appendix

Table A.1. Experimental results for 0 g/l HA concentration treated by Macro EDM

No. parameter	Discharge Current	Time-On	Time-Off	Gap Voltage	Powder Concentration	Time 1	Time 2	Time 3	Average
1	2	2	2	2	0	9.75	7.5	8.75	8.66667
2	2	5	5	5	0	16	20.75	26	20.9167
3	2	8	8	8	0	23.25	20	25	22.75
4	5	2	5	8	0	9.5	8.5	9.5	9.16667
5	5	5	8	2	0	13.25	12	14	13.0833
6	5	8	2	5	0	12	10.75	10.75	11.1667
7	8	2	8	5	0	12	13.5	9.5	11.6667
8	8	5	2	8	0	8	8	8.5	8.16667
9	8	8	5	2	0	11	17.5	17.5	15.3333

Table A.2. Experimental results for 5 g/l HA concentration treated by Macro EDM

No. parameter	Discharge Current	Time-On	Time-Off	Gap Voltage	Powder Concentration	Time 1	Time 2	Time 3	Average
1	2	2	2	2	0	6.75	9.75	7.75	8.08333
2	2	5	5	5	0	10	10.5	9.5	10
3	2	8	8	8	0	9.25	10	10.75	10
4	5	2	5	8	0	5.85	6.25	6.25	6.11667
5	5	5	8	2	0	4.75	4.25	5	4.66667
6	5	8	2	5	0	3.1	3.25	3	3.11667
7	8	2	8	5	0	6.25	7.25	8.5	7.33333
8	8	5	2	8	0	3.1	3.25	3	3.11667
9	8	8	5	2	0	3.5	3.5	3.5	3.5